Lab on a Chip

CRITICAL REVIEW

View Article Online
View Journal | View Issue

Cite this: *Lab Chip*, 2019, **19**, 3575

Microfluidics and catalyst particles

M. Solsona, †*[a] J. C. Vollenbroek,†[a] C. B. M. Tregouet, †[a] A.-E. Nieuwelink,[b] W. Olthuis,[a] A. van den Berg, [a] B. M. Weckhuysen [b] and M. Odijk [a]

Received 7th April 2019,
Accepted 6th September 2019

DOI: 10.1039/c9lc00318e

rsc.li/loc

In this review article, we discuss the latest advances and future perspectives of microfluidics for micro/nanoscale catalyst particle synthesis and analysis. In the first section, we present an overview of the different methods to synthesize catalysts making use of microfluidics and in the second section, we critically review catalyst particle characterization using microfluidics. The strengths and challenges of these approaches are highlighted with various showcases selected from the recent literature. In the third section, we give our opinion on the future perspectives of the combination of catalytic nanostructures and microfluidics. We anticipate that in the synthesis and analysis of individual catalyst particles, generation of higher throughput and better understanding of transport inside individual porous catalyst particles are some of the most important benefits of microfluidics for catalyst research.

1 Introduction

Catalysts are used in many different applications, such as fuel cells, exhaust gas catalytic conversion, water purification and chemical production amongst others. In all these fields, the physical and chemical properties of the nanostructure of solid catalysts are of great importance. Over 80% of chemicals require a solid catalyst during their production, thus the role of nanocatalysts has become crucial in order to achieve a more sustainable society.[1] The activity of these solid catalysts relies on their size, shape and accessibility of active sites. Therefore, more monodisperse and uniform catalyst materials can tremendously increase their efficiency.

During the past two decades, microfluidics has been widely used to analyse and sort micro- and nanostructures, such as cells and microparticles,[2,3] as well as to produce catalyst nanoparticles (NPs) with better control of their morphology and size.[4–7] Small volumes, high operation speeds, and small length scales in microfluidic devices give more accurate control of the synthesis parameters affecting the overall quality of the catalyst materials prepared. Although microfluidics is a powerful tool for chemical analysis,[8] its use in catalyst characterization is far from reaching its full potential. As previously done in the cell-biology field,[9] microfluidics could be an essential tool to characterize single catalyst particles at high throughput. Some critical reviews have focused on the synthesis of nanostructures using microfluidics, either as a general approach[5,6] or focused on the microfluidic principle used.[7]

In this review, we first focus on the latest advances of the microfluidic synthesis of metal and metal oxide nanocatalysts. Second, we show how microfluidics has been used for *in situ* characterization of nanocatalyst particles in terms of shape, size, activity, selectivity, and composition. Several characterization techniques working in synergy with microfluidics are discussed. After both sections we introduce the possible future applications that microfluidics can open to the heterogeneous-catalysis field. This review is intended to show an overview on synthesis and characterization, while we will highlight future opportunities enabled by the combination of both fields.

2 Synthesis

This section focuses on the most recent approaches within the last 8 years. For a more extensive overview of the synthesis of nanostructures focused on the processes taking place inside the microfluidic systems,[5] the final application[4] or the microfluidic technology used[6,7] we refer the reader to other review articles.

2.1 Metal nanoparticles

Metal nanoparticles exhibit very interesting catalytic, optical, chemical, electromagnetic and magnetic properties, all of them depending to a large degree on their size and composition. Regarding catalysis, a decrease of the NP size leads to a surface-area increase per mass, providing more active sites. Also, the surface structure is of vital importance for the NP selectivity: the presence of steps, edges or terraces in the atomic surface can influence the reaction pathways to

[a] *BIOS Lab on a Chip Group, MESA+ Institute for Nanotechnology, University of Twente, Drienerlolaan 5, Enschede, The Netherlands.*
E-mail: miguel.solsona.alarcon@gmail.com
[b] *Inorganic Chemistry and Catalysis, Debye Institute for Nanomaterials Science, Utrecht University, Universiteitsweg 99, 3584 CG Utrecht, The Netherlands*
† These authors contributed equally to this work.

favour the production of certain compounds over other products.[10,11] Therefore, colloidal synthesis procedures to prepare catalytic NPs gained increasing interest over the last few years.[12] Usually, catalytic NPs are deposited on catalyst

Table 1 Some characteristics of the synthesis of metal nanostructures using homogeneous flows (for a list of used acronyms, refer to the end of the review)

Material	Microreactor	Size	Temp.	Flow rate	Reactants	Ref.
Au NPs	Glass	11.5 nm	NS	0.05 mL min^{-1}	$HAuCl_4$ + SC + tannic acid	28
Au NPs	Silicon-glass	1 nm	NS	43.3 mL min^{-1}	$HAuCl_4$ + $NaBH_4$ + PVP	48
Au NPs	Glass capillary	48–135 nm	RT	1 mL min^{-1}	$HAuCl_4$ + AA + PVP	49
Au NRs	PTFE	≈50 nm	NS	0.1 mL min^{-1}	$HAuCl_4$ + CTABr + tannic acid + $AgNO_3$ + AA + $NaBH_4$ + PEG	50
Au NPs	PDMS	≈40 nm	NS	0.005–0.07 mL min^{-1}	Seeds + $HAuCl_4$ + AA	51
Au NPs	Stainless steel	24–36 nm	NS	0.041–3.63 mL min^{-1}	$HAuCl_4$	22
Au hollow NPs	PTFE	≈40 nm	RT	0.42 mL min^{-1}	$HAuCl_4$ + $NaBH_4$ + PVP	52
Au NPs	PDMS	≈125 nm	22–50 °C	NS	$HAuCl_4$ + PDMS curing agent	23
Au NPs	PE	2–37 nm	RT	50 mL min^{-1}	$HAuCl_4$ + SC + $NaBH_4$	30
Au NPs	PTP	NS	NS	1.7 mL min^{-1}	$HAuCl_4$ + DMSA + $NaBH_4$	53
Au NPs	Teflon and PDMS	3–25 nm	RT	10 mL min^{-1}	$HAuCl_4$ + AA + NaOH	31
Au NPs	PTE	4.3–8.7 nm	25–60 °C	0.042 mL min^{-1}	$HAuCl_4$ + dodecanethiol + ET_3SiH + THF	54
Au NPs	PTE	≈100 nm	NS	5×10^{-5} mL min^{-1}	$HAuCl_4$ + H_2SO_4	38
Au NPs	3D-printed	≈10 nm	NS	NS	$HAuCl_4$ + $NaBH_4$ + SC	47
Au NPs	PEEK	1–2 nm	100 °C	0.08 mL min^{-1}	$HAuCl_4$ + SC	14
Au NPs	Glass capillary	1.8 nm	100 °C	0.01 mL min^{-1}	$HAuCl_4$ + SC	15
Au NPs	Stainless steel or Teflon	1.5–181 nm	RT	0.2–20 mL min^{-1}	$HAuCl_4$ + AA or $NaBH_4$	55
Au NPs	Teflon	≈40 nm	RT	≈5.8–7 mL min^{-1}	$HAuCl_4$ + NaOH + glucose	40
Au NPs	Silicon-glass	≈40 nm	RT	NS	$HAuCl_4$ + SC	56
Au NPs	PVDF			50 mL min^{-1}	$HAuCl_4$ + $NaBH_4$	57
Au NPs	Low temp. ceramic	3 nm		≈0.06 mL min^{-1}	$HAuCl_4$ + $NaBH_4$ + MUA	58
Au NRs	Rotating tube	≈30 nm	RT	10–40 mL min^{-1}	$HAuCl_4$ + acetylacetone + CTAB + $AgNO_3$ + carbonate buffer	59
Ag NPs	PDMS	5–12 nm	RT	20 mL min^{-1}	$AgNO_3$ + $NaBH_4$ + AA + PVP	34
Ag NPs & fibres	PDMS	30 nm	RT	0.015–0.06 mL min^{-1}	$AgNO_3$ + OPD	27
Ag NPs	Glass capillary	3.1–9.3 nm	RT	2.5 mL min^{-1}	$AgNO_3$ + SC + $NaBH_4$	36
Ag NPs	Quartz spiral	5–40 nm	130–150 °C	1 mL min^{-1}	$Ag(NH_3)_2$ + glucose + PVP	60
Ag NPs	ETFE and PTFE	5.3–7 nm	90 °C	0.2–0.6 mL min^{-1}	$AgNO_3$ + NaOH + C. Platycladi	61
Pd NPs	Silicon-glass	1 nm	60 & 280 °C	1 mL min^{-1}	Pd acetate + toluene + methanol + OLA + TOP	62
FeZn NPs	Stainless steel	≈5 nm	30 & 150 °C	3 mL min^{-1}	$FeCl_2$ + $ZnCl_2$ + $NaBH_4$ + PVP	63
Fe_3O_4 NPs	PTFE	≈11 nm	60 °C	2.5–5 mL min^{-1}	$FeCl_2$ + $FeCl_3$ + $NaBH_4$ + PVP	16
Fe_3O_4 NPs	Hastelloy	4.9 nm	250 °C	0.19–6.6 mL min^{-1}	$Fe(acac)_3$ + anisole + (HOOC–PEG–COOH) + oleylamine	29
Cu NPs	Stainless-steel	≈10 nm	RT	0.1–40 mL min^{-1}	$CuSO_4$ + $NaBH_4$ + PVP	33, 34
Cu NPs	Teflon	135.6 nm	RT	1.8 mL min^{-1}	$CuCl_2$ + THF + $LiBEt_3H$ + SB_{12} + acetone + ethanol	64
$CoFe_2O_4$ NPs	PDMS and PTFE	5–15 nm	98 °C	NS	$CoCl_2$ + $FeCl_3$ + TMAOH	37
Ni NPs		10 nm	220 °C	2.2 mL min^{-1}	$Ni(acac)_2$ + oleylamine + octadecene + trioctylphosphine	17
Ni NPs	Stainless steel	5–9 nm	80 °C	0.1–40 mL min^{-1}	$NiSO_4$ + N_2HH_4 + PVP + NaOH	65
Ni NPs	Stainless-steel	5.3–7.4 nm	60–120 °C	3 mL min^{-1}	$NiCl_2$ + hydrazine monohydrate + NaOH + EG	66
Pt NPs	PTFE	2.8 nm	RT	0.02–0.5 mL min^{-1}	H_2PtCl_6 + PVP + HMP + UV (365 nm)	39
Pt NPs	Copper	5 nm	RT	0.84–1.7 mL min^{-1}	K_2PtCl_6 + $NaBH_4$ + PVP	67
Pt NPs	Glass	1.4 nm	0 °C	6.7 mL min^{-1}	$H_2PtCl_6NaBH_4$ + PVP	68

supports in order to stabilize them and avoid NPs clustering. These catalyst supports are porous microstructures made of an oxide and their morphology is of great importance regarding catalytic performance.[13]

Normally, the NPs and catalyst supports are produced in batch reactors with lack of controllability. Microfluidic NP synthesis uses the same reactants as batch procedures, however, with better control of the time and spatial distribution resulting in better size homogeneity.[14–17] Also, due to the smaller dimensions, heat transfer, which is dominated by conduction and convection, can be achieved in a faster manner.[18–21] Nevertheless, this comes at a price of low throughput and the development of more complex systems. Tables 1–3 show a summary of the structures, techniques, NP size, temperature and reactants used to synthesize metal nanostructures, silica and zeolites using microfluidics. As can be seen, synthesis of metal NPs starts with a metal containing salt solution and a reducing agent, although sometimes the reducing agent is not needed.[22,23] Thereafter, usually ligands or surfactants, the so-called capping agents, are used to control the shape and size of the structures. The type and mode of mixing of these ligands have a great influence on the final shape and composition of the NPs.[24] The time and contact between reagents are of great importance, both of them being better controlled by microfluidic systems. As stated in previous reviews,[5,25] microfluidic synthesis uses two different techniques to bring the reagents into contact, the homogeneous and the droplet-based approaches.

Homogeneous synthesis. Homogeneous synthesis consists of simple mixing of reagents and surfactants using usually 2 or 3 inlets which combine into a single channel,[15,26] altogether forming a Y or T shape depending on the angle of contact between the channels, see Fig. 1a. The final shape of the NPs will depend on the contact, shear between the reagents, flows and temperature,[27] see Fig. 1b. Yagyu *et al.* and Jiao *et al.* showed that the size distribution of the synthesised particles was best controlled by using smaller channels and lower flow rates.[28,29] Most of the studies reviewed synthesised nanoparticles however other shapes can be produced such as nanorods (NRs), nanostars (NSs) and nanocubes (NCs). Lohse *et al.* synthesised NRs and NCs with the same setup just by changing the flow rates of the reagents.[30] When reagents mix in a single channel, mixing occurs by diffusion. Due to the typical parabolic flow profile in microchannels, different velocities cause different residence times and consequently non-homogeneous diffusion over the channel height, Fig. 1b. Therefore, sometimes mixers are used to enhance the mixing and to provide better control of the metal NP size distribution and composition. These mixers use the inertia of the fluid to merge the reagents in a more vigorous manner[26,31,32] reducing the time of mixing to a few ms.[26] On the other hand, Fu *et al.* used the slow diffusion in homogeneous synthesis as an advantage to slow down the process and identify intermediate shapes formed during the synthesis of NPs. Typically, the synthesis is performed at room temperature, however higher temperatures are also used which can be very well controlled when integrated in the microfluidic chips. To control the contact between reagents, resulting in a better size distribution, flows can be divided into small sub-flows and then mixed together.[33–35] Also, to

Table 2 Some characteristics of the synthesis of metal nanostructures using droplets (for a list of used acronyms, refer to the end of the review)

Material	Microreactor	Size	Temp.	Flow rate	Reactants	Continuous phase	Ref.
Au NSs	PDMS	20–50 nm	NS	0.0025 mL min^{-1}	Seeds + HCl + AA + $AgNO_3$ + PVP + DMF	HFE-7500 + 2.5% Picosurf-1	69
Au NPs	PDMS	≈4 nm	RT	0.0083 mL min^{-1}	$HAuCl_4$ + BMIM-Tf_2N + methylimidazole + BMIM-BH_4	Fluorocarbon oil	70
Au NPs	PDMS	≈4 nm	RT	0.0083–0.015 mL min^{-1}	$HAuCl_4$ + methylimidazole + BMIM-BF_4	Polychlorotrifluoro-ethylene oil	71
Cu NPs	PDMS	≈10 nm	RT	0.17–0.51 mL min^{-1}	$CuSO_4$ + $NaBH_4$ + PVP + NH_3 + NaOH		72
Ag NCs	PTFE and glass capillary	30–100 nm	150 °C	0.1–0.3 mL min^{-1}	(Ag seeds) + $AgNO_3$ + PVP + EG	Air or silicone oil	73
Au NPs	PTFE and PEEK	2.5–4 nm	RT	0.087–0.7 mL min^{-1}	$HAuCl_4$ + photoinitiator + AA + PVP	PP9	74
Pd NPs	PTFE and glass capillary	8.1–9.1 nm	80 °C	0.01–0.06 mL min^{-1}	Na_2PdCl_4 + PVP + AA + KBr	Silicon oil	75
Fe_3O_4 NPs	PTFE, silicon tubing and glass capillary	3.6 nm	NS	0.067–0.6 mL min^{-1}	$FeCl_2$ + $FeCl_3$ + dextran + NH_3OH	Octadecene	76
FeMn NPs	PDMS	≈3.6 nm	NS	0.0015 mL min^{-1}	$FeSO_4$ + $MnCl_2$ + *E. coli* + PEG-PFPE	G-Oil and Abil-EM90	77
Pd NPs	PTFE and glass capillary	9–37 nm	80 °C	80 mL min^{-1}	Na_2PdCl_4 + PVP + AA + KBr	Silicon oil	78
Pt NPs	PTFE	15 nm	RT	0.175 mL min^{-1}	H_2PtCl_6 + PVP + HMP + UV (365 nm)	PP9	79
Ag NPs	PEEK and PMMA	5–20 nm	NS	0.035–1 mL min^{-1}	$AgNO_3$ + KOH	Air or kerosene	80
Au NPs	Silicon-glass	≈3–8 nm	100 °C	0.027–300 mL min^{-1}	$HAuCl_4$ + $NaBH_4$	Air, silicon oil or toluene (droplets)	81

Table 3 Some characteristics of the synthesis of bimetallic, quantum dot, silica and zeolite nanostructures using microfluidics (for a list of used acronyms, refer to the end of the review)

Material	Microreactor	Size	Temp.	Flow rate	Reactants	Ref.
$CoFe_2O_4$ NPs	PDMS and PTFE	NS	98 °C	NS	$CoCl_2$ + $FeCl_3$ + TMAOH	37
AuPd NPs	PTFE and PEEK	10 nm	NS	80 mL min^{-1}	Pd seeds + KBr + PVP + AA + $HAuCl_4$	78
AuPd NPs	Zirconia	0.9–2.8 nm	NS	43.3 mL min^{-1}	$HAuCl_4$ + H_2PdCl_4 + $NaBH_4$ + PVP	35
PtBi NPs	Capillary		260 & 350 °C	NS	$BiNO_3$ + H_2PtCl_6 + $NaBH_4$ + PVP + EG + PG	82
FePt NPs	Stainless steel	≈2 nm	120 °C	0.8–1.5 mL min^{-1}	$FeCl_2$ + H_2PtCl_6 + $SnCl_2$ + PVP + $NaBH_4$	83
Ag/CuO_2 core–shell NPs	PTFE	≈100 nm		0.25–0.5 mL min^{-1}	(Ag seeds) + $CuSO_4$ + NaOH + AA	84
CdSe NPs		5 nm	250 °C	0.42 mL min^{-1}	CdO + Se + TOP + E acid	85
CdSe NPs	PMMA	4 nm	250 °C	0.05 mL min^{-1}	CdO + Se + TOP + oleic acid	86
CdSe NPs	Capillary	3–10 nm	250 °C	0.05–0.6 mL min^{-1}	$Cd(OAc)_2$ + Se + TOP + oleic acid	87
CdSe NPs	PTFE reactor	≈3 nm	300 °C	0.6 mL min^{-1}	CdO + Se + TOP + oleic acid	88
PbS NPs	PTFE and PEEK	≈5 nm	80–150 °C	0.03–0.06 mL min^{-1}	$Pb(OAc)_2$ + TMS_2S + Se	89
SiO_2	PDMS	8 μm, 3 nm pores	RT		TEOS + CTAB + HCl + ABIL EM 90	90
SiO_2	PDMS	10–30 μm	NS	1×10^{-3} mL min^{-1}	TEOS + P123 + HNO_3	91
SiO_2	PDMS	800 nm hollow	RT	0.4 mL min^{-1}	TEOS + NH_4OH + CTAB	92
SiO_2	PDMS	34 μm	RT	16.5×10^{-3} mL min^{-1}	TEOS + P104 + ethanol + HCl	93
Zeolite A	Stainless steel and PTFE	0.9–1.5 μm	90 °C	0.2–1 mL min^{-1}	NaOH + SA + SC	94
Zeolite A	Stainless steel and PTFE	≈400 nm	90 °C	0.2–0.85 mL min^{-1}	NaOH + SA + SC	95
Zeolite A	Stainless steel and PTFE	70–1500 nm	80–100 °C	0.13 mL min^{-1}	NaOH + SA + SC	96
Zeolite A	PFPE and PFA	≈100 nm	100 °C	2×10^{-3}–5×10^{-3} mL min^{-1}	NaOH + TMAOH + TEOS	97
HKUST-1	PDMS and PFA	1–15 μm	90–140 °C	10^{-3}–0.012 mL min^{-1}	$Cu(NO_3)_2 \cdot H_2O$ + H_3BTC + EtOH + DMF	98
MOF-5					$Zn(NO_3)_2 \cdot 6H_2O$ + H_2BDC + DMF	
IRMOF-3					$Zn(NO_3)_2 \cdot 6H_2O$ + H_2BDC–NH_2 + DMF	
UiO-66					$ZrCL_4$ + H_2BDC + HCl + DMF	
HKUST-1	Digital microfluidics	5 μm		NS	$Cu(NO_3)_2$ + H_3BTC + DMSO	99

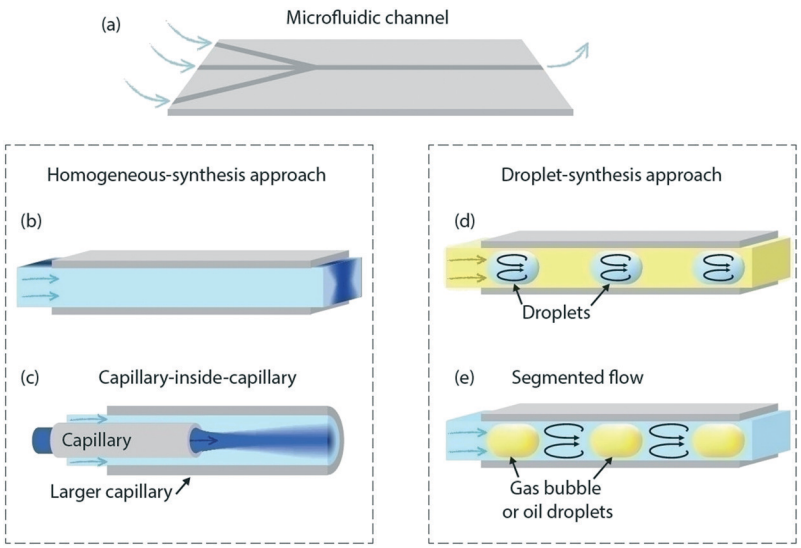

Fig. 1 (a) Schematic drawing of a typical microfluidic chip used to synthesise NPs that consists of 3 inlets and 1 main channel. (b) Main channel section where the 3 different inlets merge into a single channel. (c) Tube inside tube configuration where the contact of both reagents occurs at the centre of the big channel. (d) Droplets of similar size formed using a typical microfluidic droplet generator and (e) mixing of the segmented flows separated by gas bubbles or oil droplets.

avoid clogging of the channels due to particle agglomeration, a glass-capillary injection into a bigger tube can be used.[36,37] This technique consists of introducing a glass capillary inside a bigger channel in order to bring into contact both reagents in the middle of the channel. By doing so, the nucleation of NPs is confined in the bigger channel's centre which avoids the particles getting stuck on the walls, as shown in Fig. 1c. Alternatively, electrochemistry[38] or photochemistry[39] is sometimes used to synthesise NPs with an external trigger for the reaction. Table 1 presents an overview of the different studies found that used homogeneous flows to synthesise metal NPs. As can be seen in Table 1, the size of the NPs synthesised in microfluidic channels ranges from 1 to 181 nm with no relation to the temperature or chemicals used. The metal-containing salt coincides with the same NP materials however the reducing agent differs considerably. The reducing agent can behave as a stabilizer and therefore sometimes is not needed.[14,15] Some reducing agents are known for their toxicity, thus Ishizaka *et al.* used glucose as a more environmentally friendly reducing agent.[40] In general, the flow rates used are in the micro- to milliliter per min range which is common in microfluidic technologies and known as the main drawback for industry when trying to apply this technology. A common issue occurring during NP synthesis is the aggregation of the catalytic NPs: NPs in water tend to aggregate under the action of London forces,[41] and eventually precipitate. The classical method to prevent this phenomenon is to add surfactants or ligands to the medium. Ligands are molecules grafted or adsorbed at the interface of the NPs, which consist of polymer (or oligomer) chains soluble in the surrounding solvent that form a layer repelling the NPs from each other. Repulsion works either by electrostatic forces if the ligands are charged, or by steric forces in the case of neutral polymers.[42,43] Choosing the right ligand can be challenging and must be adapted to every situation. The choice depends on the NP's material and its environment, to ensure the stability of the polymer chains in the medium and hence of the NPs.[44] The strong effect of ligands on the final quality of the NP batch makes it one of the key factors of the synthesis. However, it has been shown that ligands can limit the catalytic activity of the NPs by covering the surface and hindering the contact between reactants and the catalyst.[44,45] Hence, the ligands must be eventually removed totally or partially from the particles before their use. Typical ligands or surfactants used are cetyltriammonium bromide (CTAB), ethylenediaminetetraacetic acid (EDTA), sodium dodecyl sulfate (SDS), polyvinylpyrrolidone (PVP), poly(ethylene glycol) (PEG) or thiols.[44,46] PDMS was the most popular material to fabricate microreactors during the early stage of NP fabrication using microfluidics,[5] however, during the last 8 years few studies have been found using this material. These have been replaced with PEEK, stainless steel or even 3D printed[47] microreactors to ensure better mechanical stability for temperature and pressure and better chemical stability.

Droplet-based synthesis. Metal NP synthesis in droplets is based on the enhanced mixing created by the droplets or segmented flows. Normally, reagents come into contact with each other in aqueous solutions and upon mixing with an organic phase either small aqueous or organic droplets are formed depending on the wetting properties of the chip, see Fig. 1d. Lazarus *et al.* used ionic liquids in order to produce NPs in droplets which opens the door to the use of many other salts and therefore other applications.[70,71] Droplet-based synthesis offers better mixing of the reagents due to the small volume of the droplets (nanoliter to picoliter regime), which is a great advantage for the particle size distribution and composition. It was demonstrated that the mixing of reagents in droplets is very sensitive to the initial formation of the droplet and that the time of mixing can be reduced down to a few ms.[100] Although mixing in droplets occurs spontaneously *via* recirculation of the liquid inside,[101] sometimes pinched, serpentine or spiral zones are introduced in order to enhance mixing.[73,75] As stated before, low throughput is one of the main drawbacks of microfluidics, however, Zhang *et al.* managed to produce large droplets (0.25 mL) by controlling the mixing inside the droplet with a counter flow mixer and therefore were able to increase the production of NPs using commercially available hardware.[78] Furthermore, using similar technology Kim *et al.* produced Pd nanocrystals with different shapes.[75] On the other hand, Xu *et al.* found that by controlling the flow rate they could control the size of Cu NPs. Frequently, droplets are formed by the aqueous phase and the space between droplets, the so-called continuous phase, forms a segmented flow which is used to mix the reagents, see Fig. 1e. This approach is found to better merge both reagents where the mixing is enhanced by the slip velocity of both phases.[81] Lee *et al.* formed hydrogel droplets that acted as cell membranes for cell extracts or NPs formed in the interior.[77] Zhang *et al.* used air as a continuous phase to synthesise silver nanocrystals, using O_2 directly from environmental air as a reagent, and the buffer space for the sub-product NO.[73] Table 2 shows an overview of the different studies found that used droplets to synthesise metal NPs.

2.2 Bimetallic NP, quantum dot, silica particle, zeolite and MOF synthesis

An overview of the synthesis of other kinds of particles such as: bimetallic NPs, quantum dots (QDs), silica microparticles, zeolites and metal-organic frameworks (MOF) is briefly mentioned but not comprehensively summarized in Table 3.

Bimetallic NPs have unique properties due to their synergetic effect on catalytic reactions. By combining two metals or metal oxides the properties of the final NPs can differ from those of the pure metal NPs of the initiators. Bimetallic NP synthesis is performed by mixing both salt solutions, providing a mixed alloy, Fig. 2a, or by controlling the deposition rate of a second metal on a seed from the first one, Fig. 2b. Some studies have shown that NPs synthesised

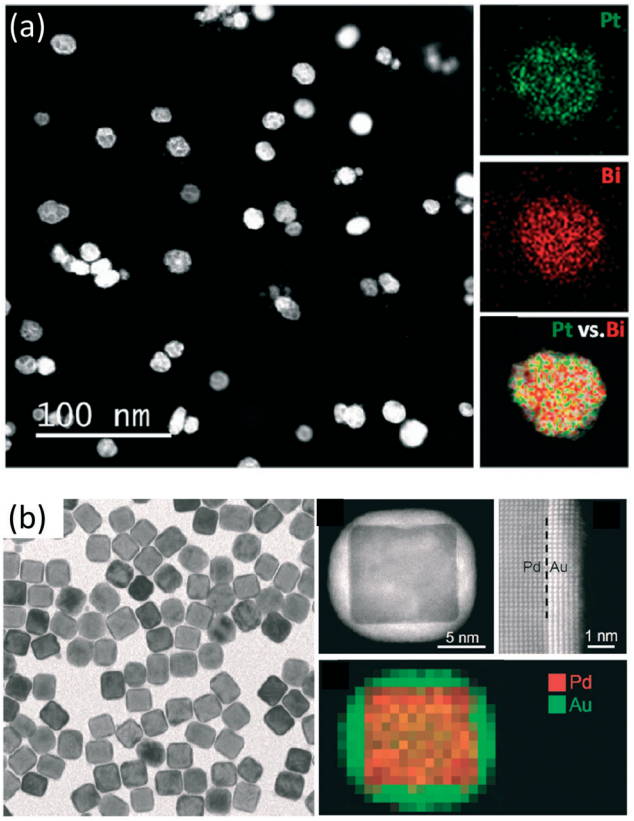

Fig. 2 (a) HAADF-STEM image and EDS element maps of PtBi intermetallic NPs. Reprinted (adapted) with permission from Zhang, D. *et al.*[216] Copyright (2015) American Chemical Society. (b) TEM image, HAADF-STEM image and EDX mapping of Pd–Au core–shell nanocrystals obtained using seeded growth of Au on the 18 nm Pd cubes. Reprinted (adapted) with permission from Zhang, L. *et al.*[217] Copyright (2014) American Chemical Society.

using microfluidic technologies have high electro- or photocatalytic activity.[82–84]

QDs are semiconductor particles smaller than 10 nm in diameter and their unique optical properties are very dependent on their size.[102] They are normally made of CdSe, CdS, InP or PbS and have been extensively synthesised using microfluidics due to the controllability enabled by this technology. As examples, Wang *et al.* could control the size and shape of QDs by using a standard microfluidic setup[88] and Lignos *et al.* could study the kinetics of PbS formation in small droplets inside a microfluidic chip.[89] QDs such as CdSe are always synthesised at high temperatures which can be very well controlled in microreactors, Table 3. Recently, a 6-step (microfluidic chip) procedure was used to fabricate different types of core–shell QDs in a very controllable and reproducible manner.[103]

To prevent aggregation of the catalytic NP dispersion inside the channel while driving catalytic reactions, catalyst supports are used to stabilize the NPs.[13] These supports are frequently made of silica, alumina or titania and they need to be very stable at high temperatures and pressures. Furthermore, they are often very porous to increase the available surface area. Various studies have synthesised porous silica microparticles,[94–97] however, not with a catalytic purpose. Bchellaoui *et al.* used droplet microfluidics to synthesise very monodisperse porous microparticles.[91] This confirms the suitability of this technology to fabricate catalyst supports.

Zeolites are another class of commonly used catalysts, due to their nanoporosity and their acidity. However, very few studies have tried to implement their synthesis in microfluidics. Indeed, depending on the type of zeolite, the synthesis conditions can vary from room temperature to high temperatures (typically 200 °C for the reaction and more for the calcination step[104]). In zeolite synthesis precise control of the synthesis conditions is important, because there are many different types of zeolites in terms of their structure. A small change in the conditions may change the structure. That is why zeolites have been synthesized at the sub-millimeter range in microfluidic chips in droplets,[94,95,97,105] but only syntheses at relatively low temperatures and short reaction times have been investigated so far. The catalytic activity of these microfluidic-synthesized zeolites has been shown to decrease the reaction time of alkyl borate synthesis by a factor of ten.[97]

Metal organic frameworks (MOFs) are crystalline structures that can be used as heterogeneous catalysts. These materials are normally porous and can contain different transition metals or functional groups which can be very suitable for catalysis.[106] Few studies have been found to use microfluidics to synthesize MOFs.[107] In this work, the authors synthesised different kinds of MOF structures claiming that the time needed could be decreased from a few hours to a few minutes by using microfluidic technologies.[98]

2.3 Conclusions

Catalyst NPs have been extensively synthesised using microfluidics. The shape and size of the particles are very dependent on the contact form and time between the different reagents. However, few studies were found where they synthesised bimetallic NPs, zeolites and catalyst supports. It has been demonstrated that microfluidic synthesis of nanostructures provides a more uniform and reproducible approach. However, low throughput seems to be the main drawback hindering the widespread adaption by industry.

Progress made in catalyst NP synthesis is realized by fine characterization methods enabling the analysis of the NPs and the quantification of their catalytic activity. Integration of these methods in microfluidic devices to analyse the NPs *in situ* could lead to fast analysis with few materials for rapid feedback on the synthesis. The next section presents recent advances in NP characterization and supported catalyst materials in microfluidics.

Whilst low throughput has always been the main drawback for industry purposes, it is possible to increase it by producing larger droplets while maintaining good control

of the system homogeneity.[78] For catalysis, no studies were found synthesizing catalyst NPs on top of catalyst supports all together in the same process. Controlling the NP location on the catalyst supports could increase the catalytic efficiency of the NPs per mass which is of great interest when dealing with noble metal materials. Also, no clear information was found regarding the selection of ligands, which play a crucial role in the synthesis of NPs. In general, if microfluidics can control the synthesis and location of NPs on catalyst supports, thereby increasing the throughput in a cost-effective manner, we foresee great potential for microfluidics in industry.

3 Characterization

3.1 Introduction

In microfluidic synthesis, *in situ* (direct) characterization can act as a fast feedback mechanism on important synthesis parameters such as the flow rate and temperature. Examples of the additional parameters that determine the success rate of NP synthesis are the size, shape, uniformity, oxidation state, activity and purity. *In situ* measurements allow for information at different stages in both time and space during synthesis or activity testing of catalyst materials. With this information, the growth rate, reaction intermediates and deactivation can be monitored[26,53,57,62,108–112] allowing for kinetic and mechanistic studies,[108,113–117] as summarized in Table 4 and illustrated in Fig. 3.

To narrow down the scope of this section, only *in situ* characterization will be discussed, and it is divided into three parts. First, characterization techniques used in microfluidics will be discussed. Second, direct characterization of NPs will be discussed, where the characterization of the shape, size, oxidation state, crystal structure and elemental composition is analysed,[26,53,57,62,118–121] as can be found in Fig. 3. Last, the activity of these NPs supported on porous materials forming packed-bed or wall-coated microreactors will be treated. Catalyst NPs are often supported on porous oxides or polymers to provide stability and prevent sintering of NPs. In the characterization of supported catalyst particles, mainly the activity and selectivity of the catalyst material are of interest. Furthermore, the dispersion and stability over time of the catalyst on the support are important.

An overview of the characterization methods found in the literature is shown in Table 4. Here, the type of reactor and the nanoparticle/support combination are listed together with the type of study, characterization and the temperature reported. In the review of Yue *et al.* 2012,[122] the combination of spectroscopy and microreactors was already discussed in great and excellent detail. In their review the working principles of various spectroscopic techniques such as fluorescence spectroscopy (FS), infrared (IR), ultraviolet-visible (UV-vis), Raman spectroscopy (RS), nuclear magnetic resonance (NMR), and X-ray absorption spectroscopy (XAS) are discussed extensively. In contrast, we will briefly discuss the working principles of the aforementioned techniques, and focus on the use of these techniques in *in situ* catalyst- and nanoparticle characterization.

3.2 Characterization techniques

Gas chromatography and mass spectrometry. To characterize the performance of a catalyst, often a reaction is monitored by looking at product formation with in-line gas chromatography (GC) or mass spectrometry (MS). With these techniques, as summarized in Table 4, the conversion and selectivity of a catalyst bed can be determined.[108,111,115,116,123–129] The main advantage of MS and GC lies in their low limit of detection and broad range of sensitivity for multiple compounds. Unexpected products or molecules can be detected, since these in-line systems do not require tuning of the system in order to detect a specific molecule or compound. However, these in-line methods are less suitable for monitoring the catalyst bed at various times or distances along the bed. This means that in combination with microfluidics they can only be used at the outlet of a system and cannot give information about on-chip processes. Moreover, short-lived intermediates cannot be detected with GC and MS. For this a broad host of microscopic and spectroscopic techniques, as summarized in Table 4, are available *i.e.* ultraviolet-visible (UV-vis), infrared (IR), Raman spectroscopy (RS), nuclear magnetic resonance (NMR), and X-ray absorption spectroscopy (XAS).[109,110,112,114,116,117,124,127,130–136] Furthermore, it is found that GC and MS are used in combination with IR or XAS,[108,116,127,129] as summarized in Table 4, to get information on both the composition of the product feed at the outlet and on the intermediates that are being formed or structural changes in the catalyst that occur from XAS and IR measurements.

Nuclear magnetic resonance. The advantage of nuclear magnetic resonance (NMR) is that it can give very detailed and specific information on organic compounds (H or C-NMR) or the coordination of an inorganic material (Al-NMR); this is due to the fact that NMR is based on oscillating electromagnetic fields that can tune into the specific resonance of atomic nuclei.[137] This specificity makes NMR a very powerful technique. However, due to the tuning of the NMR magnet, only one element can be measured at the same time; multiple NMR devices are needed to measure two different atoms simultaneously. An example of the use of NMR in microfluidic systems is given by,[112,131] where hyperpolarized hydrogen is used to polarize the reactant (propane in this case). H_2-Polarized propane has a signal-to-noise ratio 300 times larger than non-H_2-polarized propylene.[112] This was used to monitor the formation of propane from propylene. Fig. 4a shows the reactor setup from Zhivonitko *et al.* 2012.[131] Here they use a separate large encoding coil around the catalyst bed that is placed inside an 800 μm inner diameter capillary. A much smaller and more sensitive detection coil is placed at the outlet of the system to record the NMR spectrum. The outlet capillary has an inner

Table 4 Some properties of *in situ* characterization of catalysts using microfluidics (for a list of used acronyms, refer to the end of the review)

Catalyst support (reactor type)	Measured property	Analytical technique	Temp.	Reactor material	Ref.
Pt/PMMA–polyDADMAC (packed-bed)	Degradation of cochenille red with sodium borohydride	Optical/VIS: photometer	25–80 °C	Glass microtube	79
Pt/SiO_2, Au/TiO_2, silicon-glass chip and Au/Al_2O_3 (wall coated)	Bonding state and chemical state of Au/TiO_2 (XANES) – coordination numbers and bond lengths for Au/Al_2O_3 (EXAFS) – crystal structure of TiO_2 support in Au/TiO_2 (EXAFS) – intermediates and products in ethylene hydrogenation (IR and GC)	XANES, EXAFS, IR and GC	40–200 °C	Silicon–silicon chip with silicon nitride windows	108
Pt/ZnO nanorods (wall coated)	Photocatalytic activity measured with the degradation of phenol	UV-vis	NS	Fused-silica capillary	109
ZnO/TiO_2 (wall coated)	Photocatalytic kinetic performance with the degradation of methylene blue	UV-vis	NS	Fused-silica capillary	110
Rh/Al_2O_3 (wall-coated)	Oxidation state of Rh during partial oxidation of methane (XANES) – selectivity and conversion for direct partial oxidation of methane (MS)	XANES and MS	331–378 °C	Quartz capillary	111
Pt/Al_2O_3 and Pd/Al_2O_3 (packed-bed)	Propane formation from propylene and *para*-hydrogen – density of catalyst sites	NMR	NS	Capillary (not specified)	112
M–TiO_2 (M = F, Si, K, Mn, Co, Ni, Cu, Mo, and Au) (packed-bed)	Photocatalytic activity measured with the degradation of methylene blue	Optical/vis: CCD camera	NS	Glass–glass	113
TiO_2 (wall-coated)	Photocatalytic activity measured with the degradation of Rhodamine B	UV-vis	NS	Fused-silica capillary	114
Ru nanoparticles (wall-coated in polymeric matrix)	Catalytic activity by hydrogenation of various carbonyl compounds	GC-MS	<160 °C	Fused-silica capillaries	115
Au/SiO_2 (packed-bed)	Cascade dihydropyran synthesis, yield and selectivity (IR and GC) – oxidation state indicating catalyst deactivation (EXAFS)	IR, GC, and EXAFS	NS	Stainless steel plug flow reactor	116
Au nanoparticles (wall-coated)	Reduction of *p*-nitrothiophenol – influence of O_2 and H_2 on dimerization of *p*-aminothiophenol	SERS	NS	Glass–PDMS	117
Cu/ZnO (packed bed)	Activity by methanol to hydrogen conversion	GC	195–260 °C	Silicon-glass chip	123
Pt–Co/Al_2O_3 (wall-coated)	Oxidation state of Co and Co oxides (Raman) – CO conversion, O_2 conversion and CO_2 selectivity for preferential oxidation of carbon monoxide (GC)	Raman and GC	120–160 °C	Fe–Cr–Al capillary in a stainless steel tube	124
Pt thin film (catalyst spot 15 μm^2)	Catalytic activity by CO oxidation	MS	<300 °C	Silicon-glass	125
$Cu_xPd_yAu_{(1-x-y)}$ alloy surface (wall-coated)	Catalytic activity by H_2–D_2 exchange reaction	MS	27–327 °C	Glass–glass chip	126
Pd/Al_2O_3 (packed-bed)	Turn over frequency (TOF) for oxidation of carbon monoxide	FTIR and GC	250 °C	Silicon-glass	127
Pt/Al_2O_3 and Rh/Al_2O_3 (fixed-bed)	Deactivation by monitoring oxidation state during reaction (XANES) Conversion of partial oxidation of methane (MS)	XANES and MS	352 °C	Quartz glass capillary	129
Au–Pd/TiO_2 (packed-bed)	Conversion and selectivity for the oxidation of benzyl alcohol	Raman	80–140 °C	Silicon-glass chip	130
Rh/SiO_2 (packed-bed)	Turn over frequency (TOF) for propene hydrogenation with hyperpolarized hydrogen	NMR	60 °C	Capillary (not specified)	131
Pd/carbon and zeolite Y and beta (multiple particles in droplet)	Yield for the acylation of anisole	ATR-IR	20–150 °C	PFA tubing	132
PtNi nanoparticles (wall-coated)	Hydrogenation of azobenzene dye	UV-vis	NS	Photonic crystal fiber	133
Pt film (wall-coated)	Adsorption of CO on Pt film	ATR-IR	NS	Stainless steel tube	134
Au–Pt–Au NPs (suspension)	Reduction of 4-nitrothiophenol by adsorbed hydrogen	SERS	5–50 °C	Glass–glass	135
Au–Ag alloy NPs (wall-coated)	Reduction of 4-nitrophenol for kinetic study of various Au/Ag ratios	UV-vis	NS	Silicon-glass	136
TiO_2 graphene oxide (wall-coated)	Photocatalytic activity measured with the degradation of methylene blue	Optical/vis: absorbance through channel	NS	PDMS–PDMS	138
Pt/Al_2O_3 (packed-bed)	Pt dispersion in Pt/Al_2O_3 catalyst layer	CO chemisorption and GC	25–250 °C	Silicon-glass chip	148
Zeolite H-ZSM-5 (packed-bed)	Deposition and dissolution of asphaltenes in H-ZSM-5	Raman and UV-vis	NS	Silicon-glass chip	149

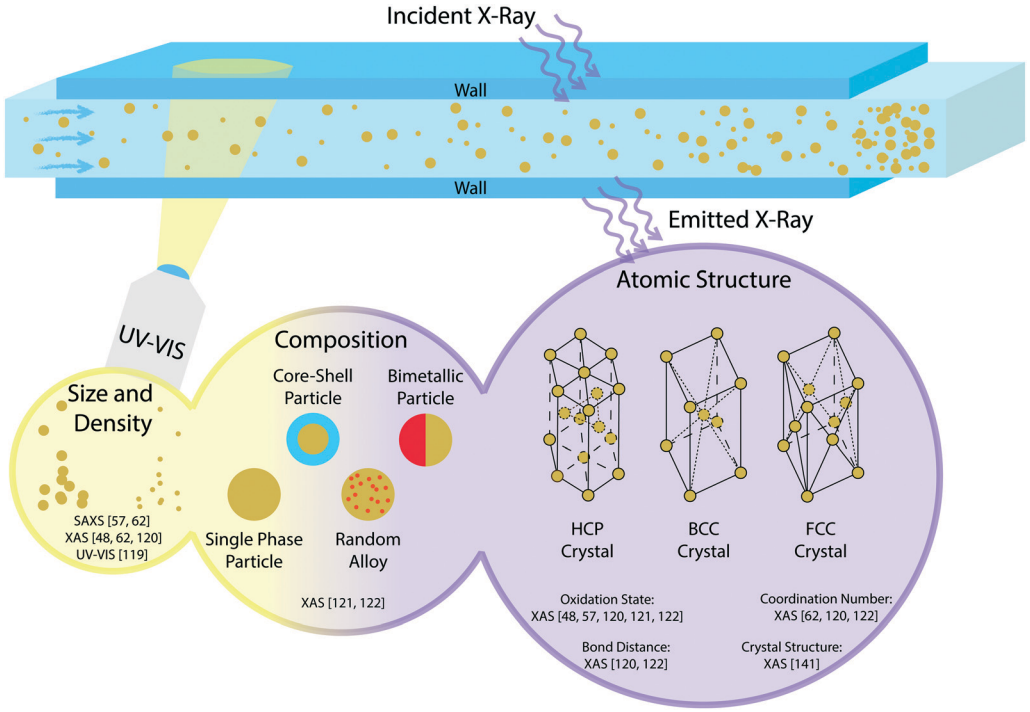

Fig. 3 Schematic overview of *in situ* characterization techniques for catalyst nanoparticle synthesis, as found in the literature, using UV-vis spectroscopy and X-ray absorption spectroscopy (XAS).

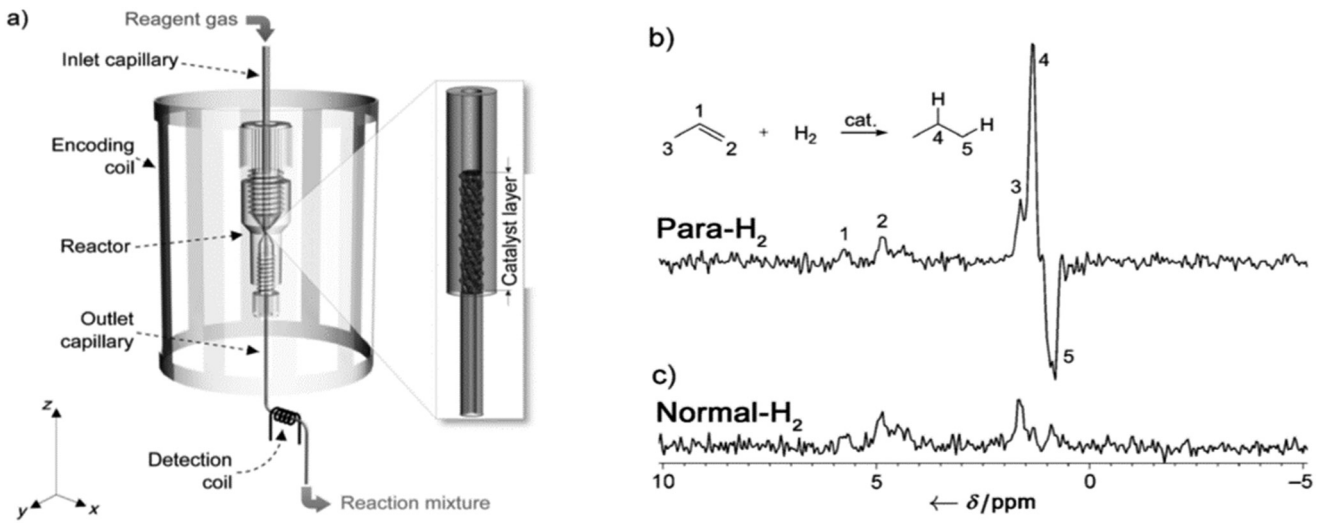

Fig. 4 a) Experimental setup. Gaseous mixture containing *para*-hydrogen and propene flows through the catalyst bed packed inside the inlet capillary close to the connection between the inlet and the outlet capillaries. Three types of capillaries of different diameters (ID 800, 405, and 150 μm) were used as the inlet capillary. The diameter of the outlet capillary was constant in all experiments (ID 150 μm). The catalyst bed was placed inside the encoding coil. b) and c) ^{1}H NMR spectra of the reaction mixture measured using the detection microcoil in the experiments with b) *para*-hydrogen and c) normal hydrogen at 22 °C. The reaction was carried out in an R-800-5 reactor. Reproduced with permission from Zhivonitko, V. V. *et al.*[218] Copyright Wiley-VCH Verlag GmbH & Co KGaA, Weinheim, 2012.

diameter of 150 μm. Fig. 4b and c show the signal enhancement when *para*-hydrogen is used.

Ultraviolet–visible spectroscopy and X-ray absorption spectroscopy. In many studies of photocatalytically active particles, the degradation of a catalyst by the de-colouring of a dye is studied. This can either be measured with a change in the UV-vis absorption spectrum[109,110,114,133] or by looking directly at the intensity of the emitted light with a photometer.[113,138] UV-vis spectroscopy uses the absorbance of light by different functional groups in molecules or inorganic structures, ranging from the ultraviolet to the visible light spectrum (200–800 nm). Depending on the size

of the conjugated system or the presence of, for example, charge transfer transitions, each compound shows a unique UV-vis absorption spectrum.[122] The advantage of UV-vis is that it is easily performed in combination with microfluidics. Transparent glass–glass reactors or tube reactors are suitable in combination with UV-vis,[109,110,114,133,136] as summarized in Table 4. The limitation here is determined by the absorption of UV-light by the glass cover, which fully absorbs wavelengths below 250 nm.[139] Moreover, absorption depends on the path length, which results in a relatively poor limit of detection for microfluidic systems, as the path length is typically smaller than in conventional setups. A hollow core crystal photonic fiber (HC-CPF), coated with PtNi NPs, was used to investigate the hydrogenation of an azobenzene dye using UV-vis spectroscopy.[133] Fig. 5 shows the setup in which they used the entire length of the fiber for measurements, obtaining a stronger signal. A disadvantage of such a system is that it reduces the temporal or spatial resolution of the data along the fiber.

X-Ray absorption spectroscopy (XAS), in particular extended X-ray absorption at fine structures (EXAFS) and X-ray absorption near edge structures (XANES), is a very powerful technique in characterizing the composition, bond distance, oxidation state, coordination number and crystal structure of nanoparticles,[26,53,57,62,108,119–121,140] as shown in Fig. 3. Disadvantages of XAS measurements are the need for an extensive database of reference samples and the time-consuming and complex data analysis that is needed to extract the desired information. Still, it can be noticed that microfluidics is much used, and actually required in XAS measurements due to the requirement of small volumes and reactor dimensions in synchrotron facilities. As an example, the microreactor used by Gross *et al.* 2014 (ref. 116) benefits from the micrometre-range channel heights, as less X-ray intensity is lost in XAS transmission mode. Furthermore, the spatial resolution of 15 μm that can be achieved with synchrotron measurements can be used to measure along multiple points in the microfluidic channels. For UV-vis it is not strictly necessary to use small volumes and reactors, although it is still an advantageous technique to combine with microfluidics,[73,109,110,114,133,136] as summarized in Table 4. Furthermore, UV-vis is a much more accessible technique, since no synchrotron facilities are required to perform measurements.

Besides monitoring the formation and growth of nanoparticles, XAS can also be used to monitor the state of catalysts during operation. Change in the chemical state, crystal structure and oxidation state gives information about the performance of the catalyst in terms of deactivation and the mechanism of the reaction,[108,111,116,129] as summarized in Table 4. This information is of importance because deactivation is a common phenomenon in catalysis.[141] More about catalyst deactivation will be discussed later in section 3.3. Fig. 6 shows an example of a typical XAS setup.[111] With this setup they monitored the oxidation state of a Rh/Al_2O_3 catalyst during the catalytic partial oxidation of methane. Fig. 7 shows the different oxidation states of the catalyst along the catalyst bed.

Infrared and Raman spectroscopy. Attenuated total reflectance Fourier transform infrared (ATR-FTIR)[131,133] and transmission FTIR[107,115,126] can also be used to monitor reaction intermediates and product formation, see Table 4. Furthermore, Fig. 8A shows the reactor and Fig. 8B presents the data obtained as an example of the use of IR spectroscopy, where reactants and products can be monitored in flow in a microfluidic reactor. Contrary to UV-vis, where the absorption is based on electronic transitions, IR spectroscopy obtains information on the vibrational modes of molecules. Atomic bonds such as N–H, O–H, and C–H bonds show vibrations in the IR spectrum.[122] IR spectroscopy can be used in the same configuration as UV-vis, meaning that an IR light source is located perpendicular to a flow channel with a detector on the opposite side. Specific wavelengths of the IR-beam are absorbed, depending

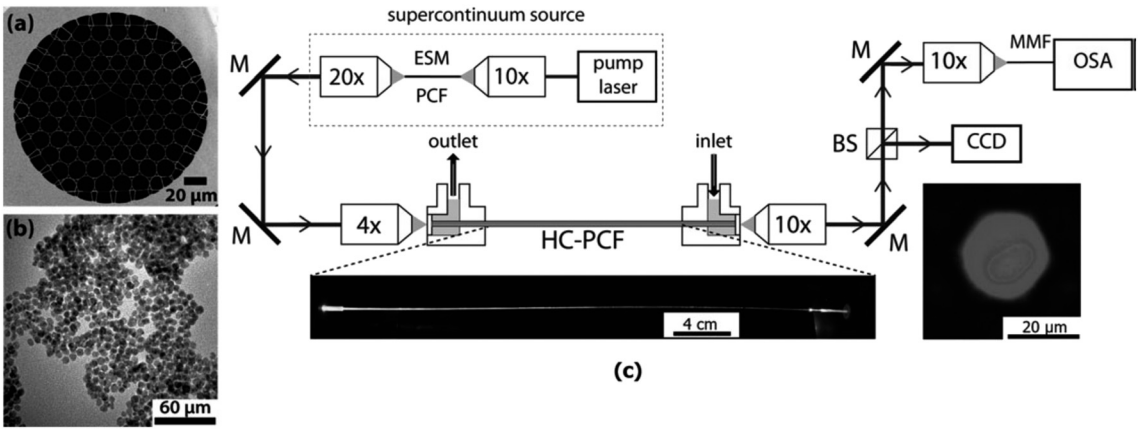

Fig. 5 a) SEM image of the Kagome HC-PCF used in the experiments, b) TEM image of 6.3 nm PtNi NPs, and c) optical setup used for the DR1 hydrogenation in particle-deposited Kagome HC-PCFs. The left photograph shows the side-view of the irradiated Kagome HC-PCF. The right photograph shows the guided mode in the core, when the fiber is filled with isopropanol and impregnated with 6.3 nm PtNi NPs. M, mirror; MMF, multimode fiber. Reproduced with permission from Ponce, S. *et al.*[219] Copyright Wiley-VCH Verlag GmbH & Co KGaA, Weinheim, 2018.

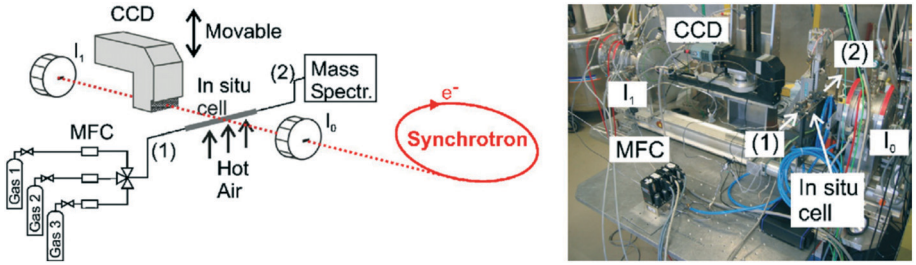

Fig. 6 Schematic setup and picture for mapping the oxidation state inside a catalytic reactor in two dimensions under reaction conditions; CCD-detector (position-sensitive detection of the X-ray absorption) and ionization chambers ("integral" X-ray absorption spectra) as well as the microreactor (*in situ* cell), oven and gas supply including MFCs (mass flow controllers) are depicted; (1) denotes the inlet of the *in situ* cell and (2) the outlet connected to a mass spectrometer (taken from ref. 111). Reprinted from Hannemann, S. *et al.*[221] Copyright (2007) with permission from Elsevier.

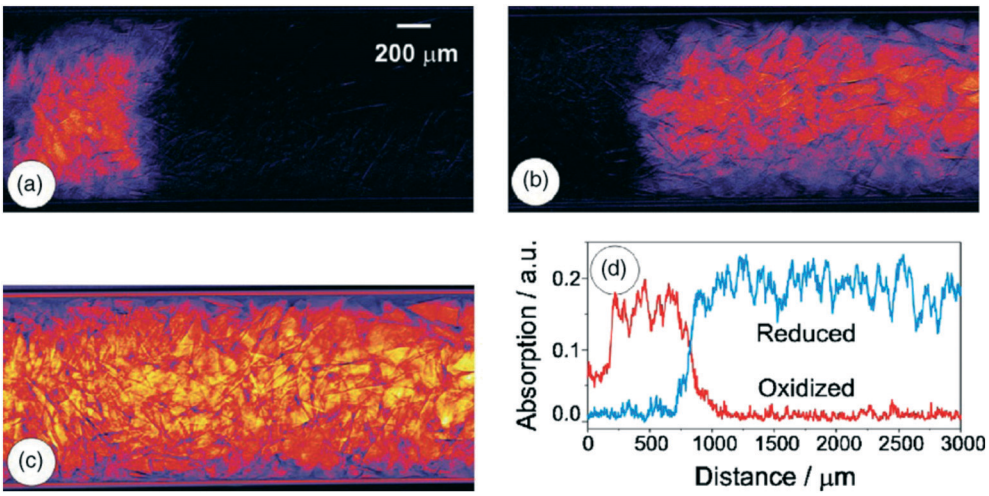

Fig. 7 Extracted components from the analysis of the 160 dark- and flat-field corrected transmission images: (a) oxidized Rh-species, (b) reduced Rh-species, (c) featureless background, and (d) relative concentration of the oxidized (red) and reduced (blue) Rh-particles in the axis of the fixed-bed (conditions: 362 °C, space velocity 1.9×10^5 h^{-1}). Reprinted from Hannemann, S. *et al.*[220] Copyright (2007) with permission from Elsevier.

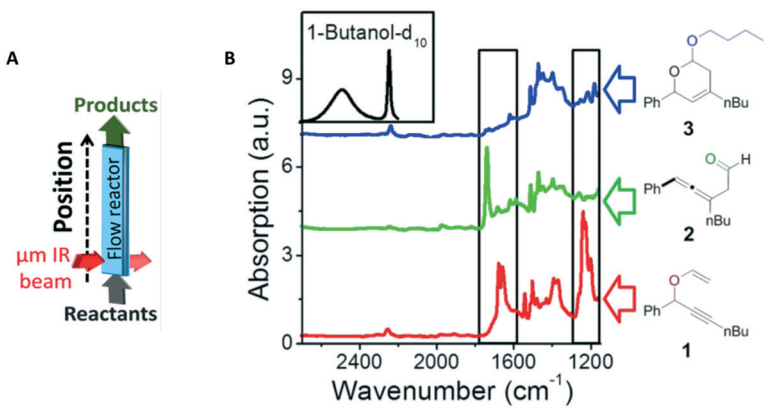

Fig. 8 (A) A scheme of the micro-IR flow reactor and (B) the FTIR spectra of the reactant, vinyl ether **1** (red), the primary product, allenic aldehyde **2** (green), and the secondary product, acetal **3** (blue). High-energy regime of IR absorption spectra of butanol-d_{10} (black), the second reactant, is shown as well. The black rectangles mark the areas in which the IR spectra of the different reactants and products can be easily distinguished from each other. Reprinted (adapted) with permission from Gross, E. *et al.*[221] Copyright (2014) American Chemical Society.

on the compounds inside the channel and due to the difference between the incoming and outgoing light, the IR absorption spectrum can be determined. An example of such a setup is shown in Fig. 5a. A different and often used IR technique couples the light source to an IR transparent crystal beyond the critical internal reflection angle. The IR-light is reflected inside the crystal, causing a small evanescent wave penetrating the surface into the liquid: attenuated total reflectance IR spectroscopy (ATR-IR). One of the difficulties of ATR-IR lies in the chip design and the total

internal reflection of an IR beam in the ATR crystal. The evanescent wave going into the sample has a small penetration depth. Therefore, the chip design has to be such that the channels are in close contact with the ATR-IR crystal. This is possible with silicon micromachining as shown in a review by Karabudak *et al.* in 2014,[142] enabling catalyst film characterization using ATR-IR in combination with microfluidic devices. Furthermore, the adsorption of gas to a catalyst film can be measured using ATR-IR.[134]

A disadvantage of using IR is the poor signal-to-noise ratio when water is used. Water itself has very broad and strong IR absorption and will likely dominate the spectrum.

A technique that allows working with water is Raman spectroscopy. Similar to IR spectroscopy, it is a vibrational spectroscopic technique. Raman spectroscopy monitors the inelastic scattering of light when interacting with a sample molecule.[122] Furthermore, Raman- and IR spectroscopy are based on different selection principles, namely polarizability and dipole moment change. This leads to both techniques being complementary to each other: vibrations that are not shown in the IR spectrum are visible in the Raman spectrum and *vice versa*.[143–145] However, Raman spectroscopy comes with its own disadvantages: spontaneous inelastic scattering typically only happens once every 10^6 photons. This makes RS signals very weak, although there are ways to enhance the signal *e.g.* by using surface enhancement structures.[117,146,147] As an example, the catalytic reduction of *p*-nitrothiophenol (PNTP) on gold NPs was performed and measured using surface enhanced Raman spectroscopy (SERS).[117] Surface enhancement takes place when compounds are in very close proximity to nanoparticles that show plasmonic resonance. In the local surface plasmon resonance field, the Raman scattering is enhanced.[135] Fig. 9A shows the reactor used in the catalytic reduction of PNTP, and the corresponding SERS spectra obtained are shown in Fig. 9B. With SERS the authors were able to calculate the rate constant for the PNTP reduction, see Fig. 9C.

3.3 *In situ* characterization of nanoparticles in microfluidic systems

For *in situ* characterization of nanoparticles, it is most important to characterize properties such as size, density, composition and atomic structure, as shown in Fig. 3. XAS is required especially for the composition and atomic structure of NPs. With XAS it is possible to probe single atoms and atom clusters. Another advantage of XAS in the characterization of synthesized NPs is the great time resolution that can be achieved. As an example, XANES was used to monitor the reduction of Au^{3+} to metallic gold within

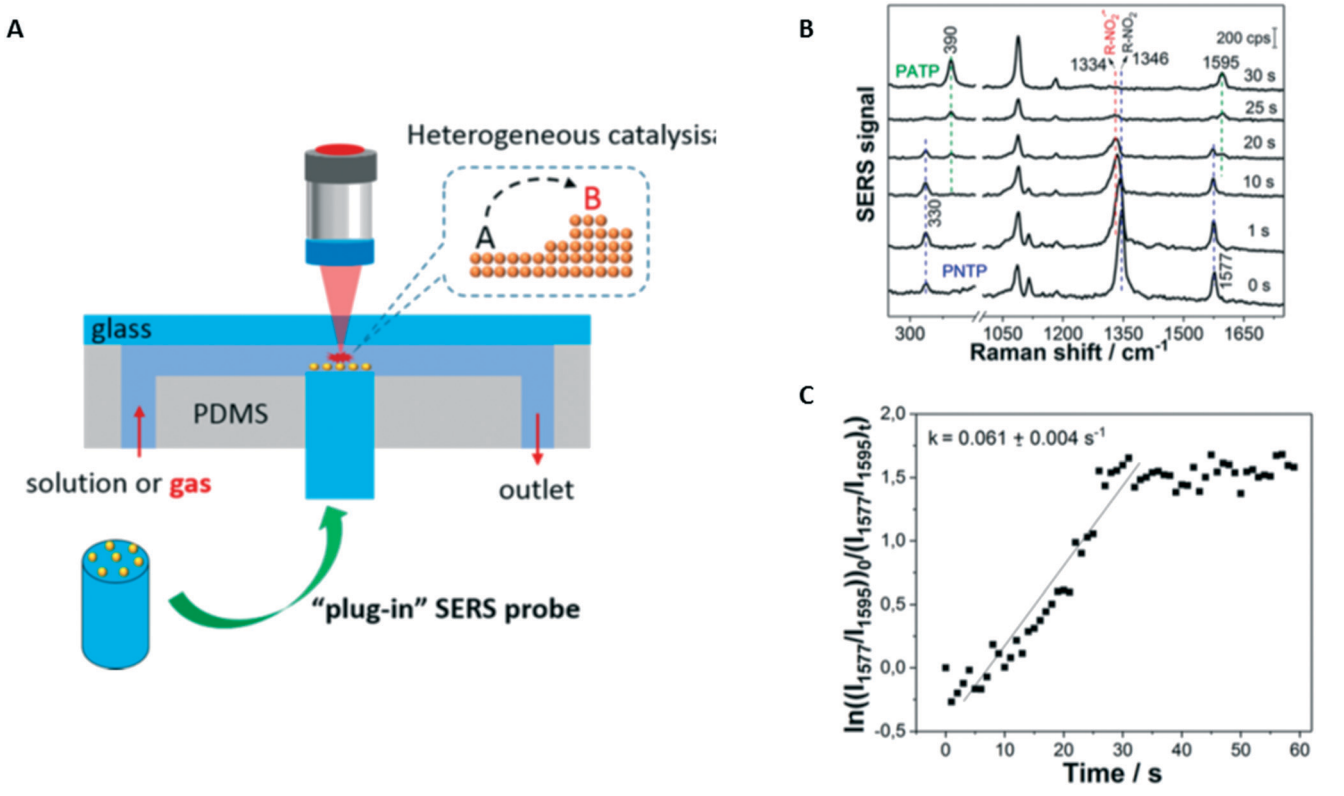

Fig. 9 (A) Schematic of the whole plug-in optofluidic platform for monitoring of nanoparticle-catalyzed reactions in a microfluidic platform. (B) SERS spectra recorded during the catalytic reduction of PNTP on immobilized gold nanoparticles in an aqueous $NaBH_4$ solution at different times. (C) Determination of the rate constant for the reduction of PNTP using the relative concentration of PNTP and PATP. Quantification is achieved by comparing the intensities of their characteristic bands at 1577 and 1595 cm^{-1} ($\lambda_{excitation}$ of 633 nm, intensity of 3 kW cm^{-2}, acquisition time of 1 s). Reprinted (adapted) with permission from Zhang, Z. *et al.*[222] Copyright (2018) American Chemical Society.

the first 2 ms of the formation.[26] With EXAFS the growth rate can be monitored by measuring the evolution of size of the formed NPs over time.[26,62]

An alternative to study the size of the synthesized NPs is UV-vis,[118] see Fig. 3. The plasmon absorption peak observed in UV-vis analysis is dependent on the size of the nanoclusters.[118] In order to characterize the size and shape small angle X-ray scattering (SAXS) can also be used.[32] It is shown that in general UV-vis data for size characterization lead to more uncertainties than SAXS analysis. However, UV-vis is much easier to use in comparison to SAXS experiments which need synchrotron facilities, as mentioned before.

An example of the setup and the UV-vis data for various sizes of synthesized Ag NPs is shown in Fig. 10. Here the shift (and broadening) of the absorbance peak can be observed for various flow rates, indicating differently sized Ag NPs.

Furthermore, it was demonstrated that the formation of atomically precise 1–2 nm-sized copper clusters could be detected using UV-vis, although no-flow conditions were used.[119] This shows the potential to use UV-vis in size characterization of NPs.[118]

3.4 Activity of supported catalyst nanoparticles in microreactors

Activity measurements of catalysts in microfluidic devices allow the study of the catalyst material under relevant conditions with well-controlled parameters such as temperature, flow rate, and pressure, see Table 4. As an example, it was previously reported that microfluidic reactors are capable of operating at temperatures and pressures up to 500 °C and 200 bar.[150–152] Catalyst activity studies are, in contrast to the NP characterization discussed earlier, conducted on supported catalyst materials. The most common types of reactors are packed-bed and wall coated reactors. Catalyst particles are either loaded on larger porous supports, this can be oxide or polymer particles,[79,112,113,116,123,127,128,130,131,148] or deposited as thin films on the reactor walls,[108–111,114,115,117,124–126,133,134,136,138] as summarized in Table 4. Examples of wall-coated and packed-bed reactors are shown in Fig. 11.[109,113,138]

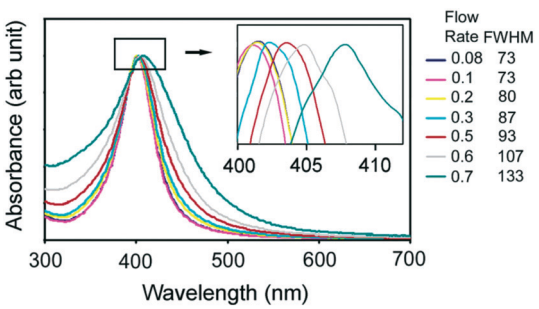

Fig. 10 UV-vis absorption spectra of silver nanoparticles made at different flow rates. Insets show the enlarged peak region (400–412 nm) and a summary of FWHMs of the absorbance of the Ag nanoparticles (in nm) at various volumetric flow rates (in mL min^{-1}) used. Reprinted with permission from Lin, X. Z. *et al.*[223] Copyright (2004) American Chemical Society.

In a packed-bed reactor, a large number of particles are used to make up the bed. This averages out the catalytic performance hindering the information at the single particle level.[127] Packed-bed reactors have a large pressure drop over the reactor bed, although an inventive solution was found[127,128] where instead of elongating the packed-bed, shorter parallel beds were used in a so-called cross-flow packed-bed reactor.

Sizes of supported NPs used in packed-bed reactors are between 20 and 120 micron as found.[113,130] Packed-bed reactors have large effective areas compared to wall-coated reactors. In packed-bed reactors, the supported catalyst material can be placed either in a microfluidic chip, often consisting of silicon–silicon,[108] glass–silicon,[123,125,127,128,130,136,148] glass–glass,[113,126,135] PDMS–glass,[117] and PDMS–PDMS,[138] or in a piece of tubing/capillary[79,109–112,114–116,124,129,131–134] to form a microreactor. All the aforementioned examples are summarized in Table 4. One of the main reasons why the characterization of heterogeneous catalysts using microfluidics is still used relatively little is the difficulty to incorporate the catalysts in the microreactor.[153] To overcome these issues, both zeolites and metal organic frameworks (MOFs) are excellent options. Zeolites are silica/alumina structures with both micro- and nanopore structures. The spatial conformation of the zeolite pores is highly dependent on their synthesis conditions, as discussed in section 2.1. Zeolites are used in acid-based (Brønsted and Lewis acid sites) catalysis. Furthermore, zeolites can be used as a support for catalytic nanoparticles, as shown in ref. 153–155, where Pt, Pd, and Cu or Ce oxides have been incorporated in a zeolite framework for heterogeneous catalytic microreactors. MOFs are highly porous structures with a very high surface to volume ratio. MOFs are built from metal ions or clusters that are linked together by organic ligands.[156] The synthesis of MOFs is very versatile where the zeolite-like, porous structure can be tuned. To date, more than a thousand structures have been synthesized.[157] In recent work, MOFs have been used inside microreactors, building both capillary reactors loaded with MOFs[157,158] and highly porous glass fiber membranes[156] and spongelike[159] supports containing MOFs in a microreactor. To the best of our knowledge, *in situ* or in-line characterization has not yet been reported with MOFs inside a microreactor. All characterization methods found were performed offline with GC.

Control of temperature both spatially and in time allows for a more detailed study of kinetics and is necessary to mimic relevant reaction conditions in large reactors. On-chip reactors have the advantage of incorporating mixing modules[135] followed by hot reaction zones, by using heater elements, on the chip.[125,150] Silicon–glass microreactors, for example, can be fabricated with integrated heaters allowing rapid and accurate control of the temperature,[123] as well as steep gradients, rapid cycling, and precise local heating,

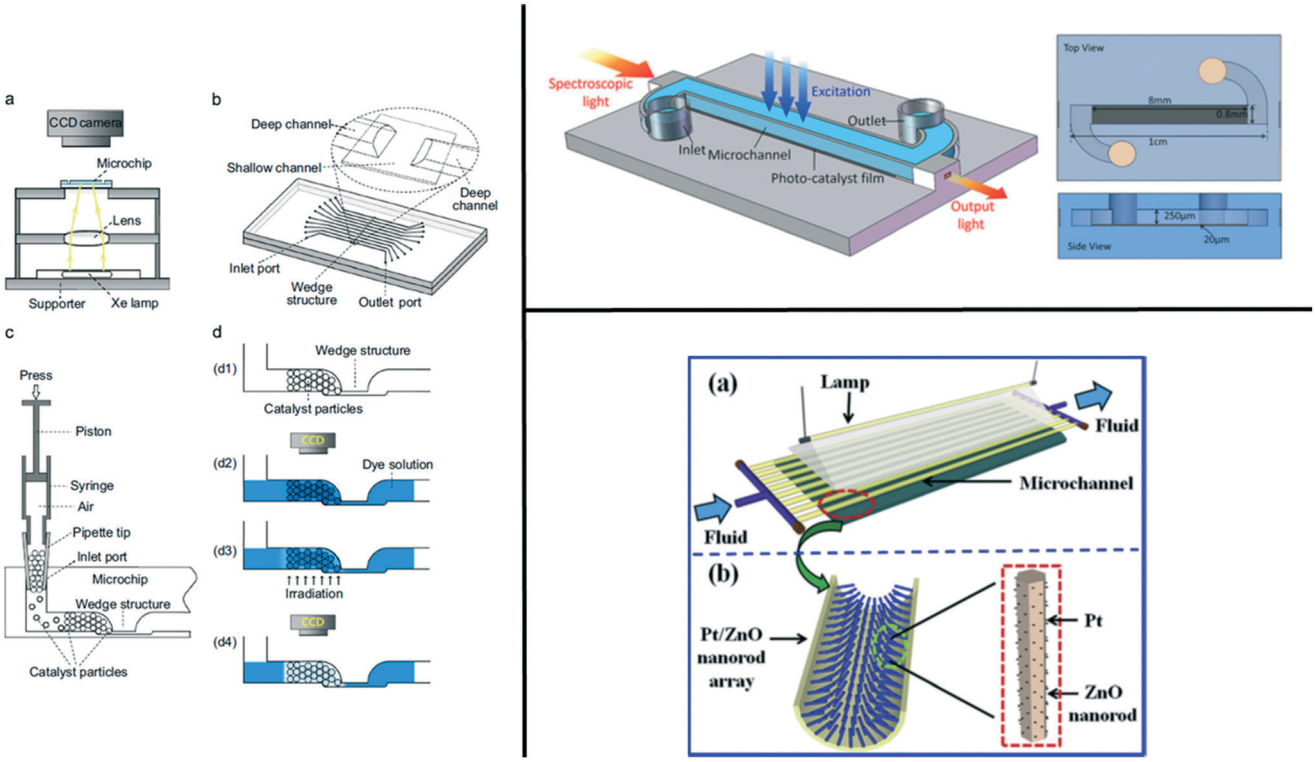

Fig. 11 Overview of the two types of reactors (packed-bed and wall-coated) on the left: a packed-bed reactor in a glass–glass reactor with (a) the setup of the microchip-based photocatalyst screening system. (b) Schematic diagram of the multi-channel array chip with a wedge structure in each channel. (c) Schematic diagram of the catalyst loading operation. (d) Illustration of the catalyst screening procedure. (d1) Loading catalyst particles in the microchannel to form the column; (d2) introducing MB solution into the channel and recording the initial channel image using the CCD camera; (d3) MB degradation under irradiation of UV-light; and (d4) recording the channel image after a definite reaction time (not to scale). Reprinted from Zhang, H. *et al.*[224] Copyright (2013) with permission from Elsevier. On the top right: a wall-coated reactor showing the schematic diagram of the fabricated microreactor. Reprinted with permission from Li, Y. *et al.*[225] Copyright (2016) Nature Scientific reports. Subject to creative commons license: https://creativecommons.org/licenses/by/4.0/legalcode. On the bottom right: a wall-coated capillary reactor with (a) the schematic diagram of the microreactor modified with Pt/ZnO nanorod arrays for photodegradation of phenol, (b) schematic diagram of Pt/ZnO nanorod arrays on the inner wall of the microreactor. Reprinted from Zhang, Q. *et al.*[226] Copyright (2013) with permission from Elsevier.

however, cleanroom facilities are needed. On the other hand, capillary reactors are simple and easier to fabricate.[79,109–112,114–116,124,129,131–134] However, external heaters, such as oil baths, electrical heaters or ovens, have to be used in combination with these capillary reactors. This makes the heating process slower when adjusting or cycling the temperature, and spatial control is lost to a certain degree.[79,124–126,130,132]

Accessibility of active sites and deactivation studies. Another parameter influencing the activity of a catalyst bed is the amount and accessibility of active sites of the catalysts. CO chemisorption, an often used bulk technique to determine acidity, was implemented in a microfluidic device for the quantitative characterization of alumina-supported Pt NPs in a high-throughput fashion.[148] Due to the strong chemisorption of CO on metal NPs, the Pt distribution in the catalyst could be determined using a silicon microfabricated packed-bed reactor. It should be noted that bulk chemisorption is considered a reliable method, but difficult to perform with smaller samples.

Monitoring catalyst activity (or deactivation) over a longer period of time can be very useful. *In situ* catalyst deactivation studies show the importance of characterization of catalysts while they are at work,[111,141,149,160] as shown in Fig. 7. However, due to the large intrinsic heterogeneities in a catalyst sample, it is not always sufficient to look at the bulk scale. Downsizing to a single particle level is very convenient and possible using microfluidics.

In situ Raman and in-line UV-vis spectroscopy were used to study the deposition and dissolution of asphaltenes in a packed-bed reactor filled with zeolite H-ZSM-5 with different silica/alumina ratios.[149] Their results show the influence of the ratio on the deposition of asphaltenes in the pore structure, as measured with Raman spectroscopy. Dissolution of asphaltenes and their aromatic sheet sizes when xylene is pumped through the zeolite pores have been measured with UV-vis, see Fig. 12.[149]

A few studies also focus on long-term catalyst performance and deactivation,[16,109–111] some of those studies extending over 100 and 120 h.[109,110] By combining synchrotron-based IR and XAS measurement, as done by Gross *et al.* 2014,[116] reactant depletion, product formation and changes in the catalyst during the reaction could be monitored.

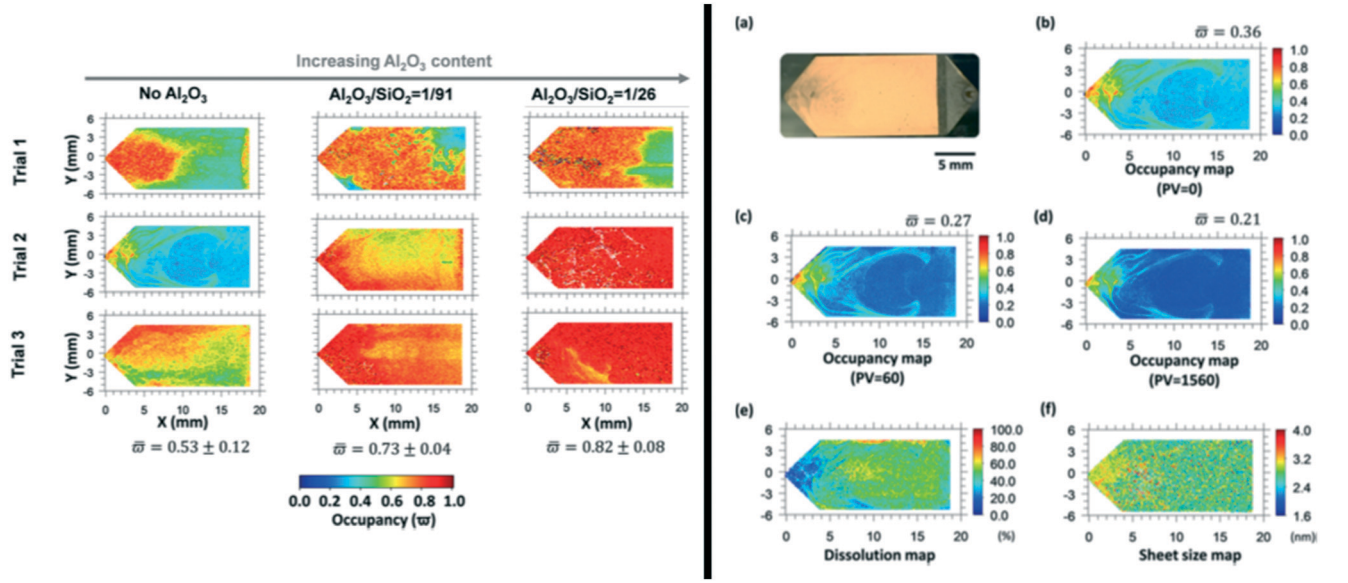

Fig. 12 On the left: occupancy maps of asphaltenes deposited within the μPBR acquired by Raman spectroscopy. Both datasets illustrate the influence of the Al_2O_3/SiO_2 ratio, showing that a higher ratio results in more asphaltene coverage indicated by the red color. On the right: (a) optical image of asphaltene deposition in the μPBR without the presence of zeolites (trial 2). Bed occupancy map of the μPBR after injection of different pore volumes of xylenes, (b) before injection of xylenes, (c) after injection of 60 pore volume of xylenes, and (d) after injection of 1560 pore volume of xylenes. The color change from light blue to dark blue in (b) to (d) indicates the dissolution of asphaltenes from the catalyst. Panel (e) shows a dissolution map, where green and red colours show areas of high dissolution and panel (f) shows a sheet size map of the aromatic asphaltene sheets between 1.6 and 4 nm. Both panels are reprinted (adapted) with permission from Chen, W. *et al.*[227] Copyright (2018) American Chemical Society.

High-throughput characterization. In order to overcome the low volume throughput of microfluidic reactors, millifluidic reactors are used (scale up), where the throughput is increased by increasing the reactor volume (increasing the channel dimensions). These reactors still have the favourable conditions of microfluidics such as: high surface-to-volume ratio, fast heat transfer, easy to vary reaction conditions and homogeneous reaction environments, but are capable of higher throughput for synthesis and characterization.[53,78,119,120,132] In addition, parallelization (scale-out) is often used in microfluidics to increase throughput.[110,113,127,128,161] Here, instead of increasing the dimensions, separate reaction channels are used to screen various catalyst compositions. Clever tricks such as the cross-flow reactor, by the group of Jensen,[127,128] do not only reduce the pressure drop over the catalyst bed but also increase the throughput. Finally, a high-throughput screening platform is demonstrated where foil forms a $Cu_xPd_yAu_{\{1-x-y\}}$ alloy surface with 100 isolated catalyst regions with different catalyst compositions.[126] Each of the regions is individually addressable and products produced at each spot after a H_2D_2 exchange reaction can be coupled to a MS. The nozzle of the MS can rapidly move between the 100 channels sampling products from all channels sequentially within 10 minutes,[126] as shown in Fig. 13.

3.5 Characterization method overview

In Table 5 an overview of various characterization methods, namely infrared, UV-vis, Raman, gas chromatography (GC)-mass spectrometry (MS), X-ray absorption spectroscopy (XAS), and nuclear magnetic resonance (NMR), and their use in combination with microfluidics is listed. These methods have been explored to investigate reaction intermediates and process yields, as well as selectivity, activity and stability of catalyst materials. Key features, such as speed, spatial resolution and chemical information obtained, are listed, and the foreseen limitations and their compatibility with microfluidics are stated.

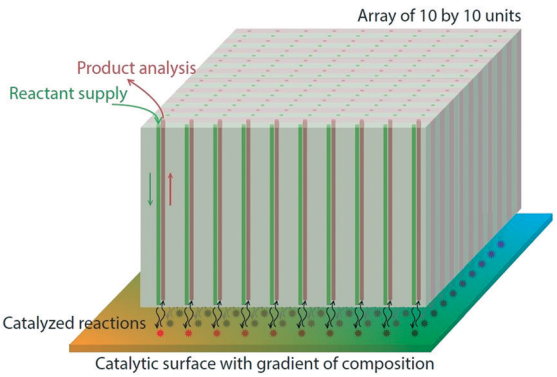

Fig. 13 Simplified presentation of the device developed by Kondratyuk *et al.*[126] to analyze catalytic activity simultaneously in 100 locations with high spatial resolution (100 measurement points on 1 cm^2). This image is based on the work from ref. 126.

Table 5 Overview of the properties of different characterization methods that can be used in microreactors

Key feature	Infrared	UV-vis	Raman	GC/MS	XAS	NMR
Speed[a]	Scan speed of 400 Hz for FTIR with a quantum cascade laser[162]	Scan speed of 0.5 Hz (ref. 163)	Scan times of 30 ms for coherent anti-Stokes Raman scattering (CARS) up to 100 s (ref. 164)	On-line analysis can go up to 650 scans/s (ref. 165)	Reported speeds from ~10 fs to ms (ref. 166 and 167)	Broad range of scan rates possible from the nanosecond to second range[168]
Spatial resolution[b]	~3 μm up to mm range[169]	~1 μm up to mm range[169]	~0,5 μm for coherent anti-Stokes Raman scattering (CARS)[169]	N.A.	15 nm–15 μm (ref. 116, 129 and 169)	Ranging from mm (ref. 131) to ~20 μm (ref. 112)
Chemical information	Chemical compound information by probing intra-molecular vibrations	Chemical compound information *via* electronic transitions	Chemical compound information by probing intra-molecular vibrations	Chemical composition of feed	Chemical compound information *via* bond distance, oxidation state, coordination number, and chemical elemental information	Chemical compound information *via* chemical shifts of elements present and the relative magnetic interactions between them
Limitations	Incompatible with water. Limited to several types of chemical bonds	Incompatible with borosilicate due to absorption of light; molecular fingerprinting is difficult to broad overlapping absorption bands	Low efficiency of normal Raman scattering (no SERS or CARS) results in long scanning times[164]	No operando or *in situ* information possible. Only outlet products can be analyzed Minimum sample volume needed	Synchrotron facilities needed, although lab-based XAS methods are becoming increasingly popular Complex data analysis	Some nuclei require long acquisition times
Compatibility	+ Good compatibility with microfluidics working with water makes the choice of solvents more limited.	+ Good compatibility with microfluidics. The scan time needed for a clear signal. Working in flow or droplets can influence this.	+ Good compatibility with microfluidics. Often enhancement is needed to obtain a large enough signal on chip. Enhancement also reduces scan speed and improves temporal information	− The need for relatively large sample volumes and the fact that only outlet products can be analyzed make it not always useful, although still detailed and valuable information can be obtained	+ Good compatibility due to small reactor volumes	+ H-NMR mostly used and compatible due to longer scan time needed for other types, such as C-NMR

[a] Typical speeds given in reviews. Please note that the speed is also dependent on the concentration that is used and the sensitivity of the machine. [b] Typical spatial resolution reported depending on the combination of chemical information needed and the catalyst material.[169]

3.6 Conclusions

Currently, it has been shown that many analysis techniques are available to characterize both catalyst nanoparticles and supported catalyst materials *in situ* in a microfluidic device. For analysis of formed products at the outlet of a microreactor often GC and MS are used. The limit of these techniques, however, is that no information along the length of the reactor can be obtained. Short-lived intermediates which only exist close to the catalyst cannot be detected with these techniques. In order to study the catalyst performance at multiple spots in a microreactor, *in situ* spectroscopic techniques such as UV-vis, IR, RS, NMR, and XAS are used.

For nanoparticle characteristics such as size, growth, and composition XAS and UV-vis are used, where mostly XAS is used to characterize the crystal structure, oxidation state, bond distance, and coordination number.

Characterization of the activity and deactivation of the supported catalyst material is mostly conducted in packed-bed reactors with multiple particles producing ensemble averages. The observed techniques are well suitable in combination with microfluidics. Locally formed products, differences in activity along a catalyst bed, turnover frequencies, and even the chemical state of the catalysts themselves are measurable using these techniques.

4 Conclusions and perspectives

Microfluidics has been used to enhance the control over chemical and physical conditions during catalytic NP synthesis. The ability to precisely control the temperature and reactant concentrations has led to very homogeneous particle synthesis in terms of shape and composition, especially for metallic particles. However, little has been done in microfluidics regarding bimetallic and zeolite nanoparticles, and regarding the integration of catalyst NPs in supporting microparticles.

Progress in synthesis is coupled with the advances in characterization. The activity of supported catalysts is often studied with GC or MS at the output of the microfluidic chip, but the use of spatially resolved methods enables the detection of short-lived intermediates which exist only close to the catalyst. UV-vis analysis and XAS are also used to measure the physical and chemical characteristics of the catalyst NPs such as the size, composition, crystal structure or coordination number. If the NPs are fixed in a packed bed, these methods also enable the study of the activity and deactivation of the catalyst NPs.

The recent development of microfluidic tools opens new perspectives for synthesis and characterization of catalytic NPs, and also to study the coupling between convection, reaction and diffusion in the complex structures that are industrial catalytic porous microparticles. These perspectives are presented in the next sections.

4.1 Future perspectives on particle synthesis

As stated in the first part of this review, using microfluidics for particle synthesis is far from its full potential. This section tries to foresee the future paths of microfluidics as a tool to synthesise catalyst NPs and other catalytic structures such as zeolites or catalyst supports.

Particle size and structure. Although it makes the mixing slightly more challenging, it is usually beneficial to work with smaller volumes to enhance the control over the experimental conditions.[170] Microfluidic droplet-based synthesis could therefore be improved by using smaller droplets: from the typical nanoliter droplet range (diameter 100 μm) to the picoliter range (diameter 10 μm) and even to the femtoliter range (diameter 1 μm). Different devices have been developed to produce picoliter droplets such as a step emulsification system,[171] or the so-called nebulator.[172] The typical microfluidic tools for droplet control can also be miniaturized to manipulate these picoliter droplets.[173] The main challenge for the miniaturization arises from the modification of the balance between surface and bulk forces: decreasing the volume of spherical droplets by a factor of 10^3 leads to a decrease of the volume forces by the same factor but the surface forces only by a factor of 10^2.

Bimetallic NPs have been shown to have great potential for catalysis. It is known that the structure and the arrangement of the two metals have a great impact on the catalytic properties of such NPs,[174] and that very precise assembly is possible when the synthesis conditions are controlled.[175] Therefore, the use of calibrated microfluidic droplets as microreactors could enable very fine control on the synthesis conditions and hence on the final size and structure of such particles to optimize their catalytic activity.

Zeolites used in the industry often require high temperatures and long reaction times and their synthesis has not been fully investigated in microfluidics yet. Moreover, the model conditions offered by microfluidics could enable a precise study of the effect of mass and heat transfer on the zeolite structure that could be later used to optimize batch synthesis.

A controlled porosity of the catalyst support is essential to enable an increase of the contact area with the reaction media while preserving an efficient mass transfer through the pores. The control of the substrate porosity can also be further improved by implementing microfluidic methods that have been shown to be efficient for bulk materials. The first method to produce such a porous medium consists of triggering a chemical reaction which produces gas and solidifies the reaction media.[176] Despite its simplicity, this method offers poor control on the pore size and structure. The second method presented here is the use of NPs as a template that are later dissolved to pattern the material.[177] In this approach, the pores consist of the space that was previously occupied by the particles, and are therefore easy to control. Compact assemblies of NPs can indeed be produced inside droplets to obtain spherical assemblies of controlled size and morphology.[178] This approach seems promising to yield microparticles with controlled porosity and high contact area with the external media. The third approach presented is based on complex liquids that can be solidified during the process of phase separation to obtain a material exhibiting a continuous network of pores of controlled size.[179] The conditions of phase separation leading to continuous pore networks, referred to as "spinodal decomposition", have been implemented in microfluidic devices to produce porous fibres and particles stabilized by NPs of silica adsorbing at the interface.[180] Such binary systems, called "bijels", experience a phase separation and are stabilized by NPs. The bottom-up approaches that rely on particle assembly or phase separation require a high level of control over the chemical and physical conditions. These conditions must indeed be homogeneous and reproducible, which calls for smaller reactors, as microfluidics can offer.

High throughput synthesis. A usual bottleneck for microfluidic devices is their throughput: smaller sizes bring better control but also naturally lower volumes produced. One of the main challenges of miniaturization is therefore to maintain the throughput. This is usually achieved by scaling out, parallelizing, the devices for droplet production and analysis.

Parallel microfluidic channels tend to interact with each other due to the variation of the pressure along the channels,[181] leading to varying flow rates and non-uniform droplet generation. However, chips have been recently developed to parallelize the production of droplets with good monodispersity by minimizing the flow rate variation[182] or by using emulsification processes that do not depend on the flow rate.[183–185] With this technology, relatively large quantities of catalysts could be synthesized with optimal control of the reaction conditions, which could be used to synthesise NPs or catalyse reactions in microfluidic reactors.

4.2 Perspectives on catalyst characterization in microfluidics

Biology has found in microfluidics an efficient way to study individual cells from large populations.[186] By isolating individual cells in single droplets, they can be characterized individually at high throughput, allowing the analysis of large samples without losing the information about each cell. Several reviews focus on droplet-based microfluidics[187] and its applications to biology, chemistry and nanotechnology.[188] The need of biologists for analysis of individual elements in a large sample is very similar to the necessity for chemists to follow the evolution of individual catalyst particles. Although nanocatalysts are considerably smaller than cells, they are often embedded in porous microparticles with sizes from one to a few tens of micrometers, such as fluid catalytic cracking particles,[155] or olefin polymerization catalysts. Under these conditions, some parallels can be made between cell analysis and catalyst analysis. Some microfluidic tools that have been developed for biology and could be used for catalysis are presented in the next sections.

Single particle analysis. In biology, to analyse the chemical content of droplets containing cells, optical detection of fluorescent molecules is currently by far the most commonly used method.[189–197] Droplets contain a fluorescent dye that is activated by a product of the cell activity, and therefore visible only if the cell is active enough, enabling a direct readout of every cell activity. The same approach has also been used to encapsulate enzymes and to measure their activity in a large number of different chemical environments.[198] Impedance-based measurements also showed promising results to analyse the content of droplets.[199] These methods could be almost directly transposed to the study of the activity of individual catalyst particles by isolating them in different droplets.

Single particle sorting. Usually in biological analysis, the droplets and the cells that they contain are sorted into two or more categories based on the results of the aforementioned analysis. The droplets identified as containing highly active cells are sorted for further analysis.[189–191,194,195,197] This could also be very useful for catalysis, for instance to select the most efficient catalysts of a population. The sorting is active, which means that the fluorescence signal is captured and triggers an actuator that reroutes the specific droplets in a different channel. These actuators can be based on various phenomena, but the most commonly used are electric field,[191,197,200] mechanic valves,[189,190,194,201] temperature,[202,203] acoustic waves,[204] pressure,[195,205] and magnetic field.[206–208]

Particle storage and tagging. Catalyst deactivation over time is of great concern for researchers and industry. The study of this phenomenon is challenging since it requires monitoring of the same particle over a long period of time, and this for a large number of particles to obtain statistically relevant data. The individual analysis of a large population of particles is a challenge for which microfluidics is well adapted. However, microfluidic systems are usually characterized by short residence times, a solution must thus be found to study these long processes.

Very similar challenges were addressed in biology and thus, different solutions were developed. The classical method consists of isolating cells in different droplets to facilitate their manipulation, storage and analysis. Moreover, for cells as for catalyst particles, evolution can be slow and observation of significant variations can require a long time.

For very long-term processes, droplets containing cells/particles can be extracted from the chip, incubated and injected into a new one later.[196] However, when possible, in order to limit the transfer of the emulsion between chips, droplets are stored directly inside the systems.[197]

In some cases, it can be interesting to vary the chemical composition of the droplets to screen various incubation conditions. It is then necessary to identify the different droplets to monitor the individual evolution of the cells/aging of the particles. To keep track of droplets, microscopic tags have been developed to enable later reading of their content and correlate the different measurements performed over time.[108,192,209–211]

It has also been shown that by confining the droplets in a line in capillaries or tubing, it is possible to keep track of the content of each droplet without tagging them and individually access them. This has been used for instance to study the proliferation of different cell populations over time.[212] Finally, droplets can also be trapped with some obstacles inside microfluidics chips, which enables an accurate knowledge of the position of every droplet.[194]

It must be noted here that an important difference between cells and particles is their density: while cells have a density close to water, catalyst particles are significantly denser and therefore settle faster, which can lead to clogging of the channels. Nevertheless, these studies of cells pave the way toward the analysis of individual catalyst particle ageing.

Parallelization. In biology as in catalysis, increasing the frequency of analysis is necessary to study larger samples. This is crucial in order to observe rare events or to find the optimal experimental conditions. This speed increase can first be achieved with pressure to increase the flow rates, and often better equipment. This can also be achieved by parallelizing the analysis process. Increasing the rate of analysis is often limited by the acquisition speed of high-speed cameras, the processing time of the computers and the maximum pressure that the microfluidic chip and connectors can withstand. However, it has been shown that catalytic activity measurements could be performed locally with a high spatial resolution on a catalytic substrate of which the composition depends on the position, to investigate rapidly the influence of the catalyst composition.[126] Fig. 13 shows a schematic of high-throughput catalyst screening with this method as has been shown in the Characterization section.

4.3 Perspectives for fundamental understanding

The structure of industrial catalyst particles is complex and consists of various necessary properties such as: porosity,

mechanical stability and catalytic activity of the particles.[213] The mass and heat transfers inside these particles and the reaction medium are only partially understood yet. Further studies are limited by the difficulty of analysing single catalyst particles during reactions.

An in-depth understanding of the mass and heat transfers inside the particles could be reached by studying model assemblies of their main constitutive elements. A 2D model network of pores and catalysts could be incorporated inside a microfluidic chip to control the input reactants and analyse the product output. This could enable the mapping of the temperature and product concentration inside the pore network. A similar approach has been used to study the phenomenon occurring when oil is pushed out a porous soil by water. A model network of pores was built inside a microfluidic chip, allowing direct observation of the phenomena occurring during oil recovery.[214,215] However, to our knowledge such a method has not been transposed to the study of transport inside the pores of catalyst particles yet.

5 Outlook

All the progress of the last decades in the field of catalyst synthesis and on-chip material characterization brought a lot of new perspectives to obtain better control over catalyst material synthesis and their function. The advantages of microfluidics in terms of chemical engineering could be used to further improve the control over the nanostructure and porosity of catalyst materials. Moreover, the tools that could enable the synthesis in even smaller droplets were presented and it was illustrated how parallelization of the devices could maintain the throughput despite the smaller size of the reactors. Based on the development of single-cell microfluidic analysis, sorting and long-term deactivation studies of individual catalysts seem to be within reach. Finally, a fundamental approach inspired by the work on enhanced-oil-recovery could enable an in-depth understanding of the mass and heat transfer in reactive porous media constituting heterogeneous catalyst particles.

6 Acronyms

NPs stands for nanoparticles, NSs for nanostars, NRs for nanorods, NCs for nanocubes, RT for room temperature, NS for not-specified, AA for ascorbic acid, SC for sodium citrate, SA for sodium aluminate, PVP for poly(*N*-vinyl-2-pyrrolidone), THF for tetrahydrofuran, CTABr for cetyltrimethylammonium bromide, BMIM-Tf2N for 1-butyl-3-methylimidazolium bis(triflylmethyl-sulfonyl)imide, BMIM-BF4 for 1-butyl-3-methylimidazolium tetrafluoroborate, BMIM-BH4 for 1-butyl-3-methylimidazolium tetrafluoroborate, TEOS for tetraethyl orthosilicate, CTAB for cetrimonium bromide, DMF for *N*,*N*-dimethylformamide, SB12 for propane-sulfonate, OPD for *o*-phenylenediamine, MUA for 11-mercaptoundecanoic acid, PEG for polyethylene glycol, TEG for triethylene glycol, EG for ethylene glycol, PDMS for polydimethylsiloxane, EFTE for ethylene tetrafluoroethylene, EA for ethyl acetate, PTFE for polytetrafluoroethylene, PFA for perfluoroalkoxyalkane, PVDF for polyvinylidene fluoride, MHA for mercaptohexanoic acid, and PP9 for perfluoromethyldecalin.

Conflicts of interest

There are no conflicts of interest to declare.

Acknowledgements

This work was supported by the Netherlands Centre for Multiscale Catalytic Energy Conversion (MCEC) an NWO Gravitation programme funded by the Ministry of Education, Culture and Science of the government of the Netherlands.

References

1 G. Centi and R. van Santen, *Catalysis for Renewables: From Feedstock to Enerly Production*, Wiley-VCH, Weinheim, 2007.
2 D. R. Gossett, W. M. Weaver, A. J. MacH, S. C. Hur, H. T. K. Tse and W. Lee, *et al.*, Label-free cell separation and sorting in microfluidic systems, *Anal. Bioanal. Chem.*, 2010, **397**, 3249–3267.
3 I. V. C. Wyatt Shields, C. D. Reyes and G. P. López, Microfluidic cell sorting: a review of the advances in the separation of cells from debulking to rare cell isolation, *Lab Chip*, 2015, **15**, 1230–1249.
4 N. Hao, Y. Nie and J. X. J. Zhang, Microfluidic synthesis of functional inorganic micro–/nanoparticles and applications in biomedical engineering, *Int. Mater. Rev.*, 2018, **63**, 1–27.
5 S. Marre and K. F. Jensen, Synthesis of micro and nanostructures in microfluidic systems, *Chem. Soc. Rev.*, 2010, **39**(3), 1183–1202.
6 Y. Song, J. Hormes and C. S. S. R. Kumar, Microfluidic synthesis of nanomaterials, *Small*, 2008, **4**(6), 698–711.
7 G. Luo, L. Du, Y. Wang, Y. Lu and J. Xu, Controllable preparation of particles with microfluidics, *Particuology*, 2011, **9**(6), 545–558.
8 K. S. Elvira and A. J. deMello, The past, present and potential for microfluidic reactor technology in chemical synthesis, *Nat. Chem.*, 2013, **5**(11), 905–915.
9 T. A. Duncombe, A. M. Tentori and A. E. Herr, Microfluidics: Reframing biological enquiry, *Nat. Rev. Mol. Cell Biol.*, 2015, **16**(9), 554–567.
10 G. A. Somorjai and J. Y. Park, Molecular factors of catalytic selectivity, *Angew. Chem., Int. Ed.*, 2008, **47**(48), 9212–9228.
11 K. An and G. A. Somorjai, Size and Shape Control of Metal Nanoparticles for Reaction Selectivity in Catalysis, *ChemCatChem*, 2012, **4**(10), 1512–1524.
12 P. Mäki-Arvela and D. Y. Murzin, Effect of catalyst synthesis parameters on the metal particle size, *Appl. Catal., A*, 2013, **451**, 251–281.
13 A. M. Gadalla and B. Bower, The role of catalyst support on the activity of nickel for reforming methane with CO2, *Chem. Eng. Sci.*, 1988, **43**(11), 3049–3062.

14 J. Ftouni, J.-S. Girardon, M. Penhoat, E. Payen and C. Rolando, Gold nanoparticle synthesis in microfluidic systems and immobilisation in microreactors designed for the catalysis of fine organic reactions, *Microsyst. Technol.*, 2012, **18**(2), 151–158.

15 J. Ftouni, M. Penhoat, A. Addad, E. Payen, C. Rolando and J.-S. Girardon, Highly controlled synthesis of nanometric gold particles by citrate reduction using the short mixing, heating and quenching times achievable in a microfluidic device, *Nanoscale*, 2012, **4**(15), 4450–4454.

16 S. Lin, K. Lin, D. Lu and Z. Liu, Preparation of uniform magnetic iron oxide nanoparticles by co-precipitation in a helical module microchannel reactor, *Biochem. Pharmacol.*, 2017, **5**(1), 303–309.

17 E. J. Roberts, S. E. Habas, L. Wang, D. A. Ruddy, E. A. White and F. G. Baddour, *et al.*, High-Throughput Continuous Flow Synthesis of Nickel Nanoparticles for the Catalytic Hydrodeoxygenation of Guaiacol, *ACS Sustainable Chem. Eng.*, 2017, **5**(1), 632–639.

18 P. S. Lee, S. V. Garimella and D. Liu, Investigation of heat transfer in rectangular microchannels, *Int. J. Heat Mass Transfer*, 2005, **48**(9), 1688–1704.

19 G. L. Morini, Single-phase convective heat transfer in microchannels: A review of experimental results, *Int. J. Therm. Sci.*, 2004, **43**(7), 631–651.

20 P. Rosa, T. G. Karayiannis and M. W. Collins, Single-phase heat transfer in microchannels: The importance of scaling effects, *Appl. Therm. Eng.*, 2009, **29**(17–18), 3447–3468.

21 B. Palm, Heat transfer in rectangular microchannels, *Microscale Thermophys. Eng.*, 2001, **5**, 155–175.

22 Á. I. López-Lorente, M. Valcárcel and B. Mizaikoff, Continuous flow synthesis and characterization of tailor-made bare gold nanoparticles for use in SERS, *Microchim. Acta*, 2014, **181**(9–10), 1101–1108.

23 H. SadAbadi, S. Badilescu, M. Packirisamy and R. Wüthrich, Integration of gold nanoparticles in PDMS microfluidics for lab-on-a-chip plasmonic biosensing of growth hormones, *Biosens. Bioelectron.*, 2013, **44**(1), 77–84.

24 A. Heuer-Jungemann, N. Feliu, I. Bakaimi, M. Hamaly, A. Alkilany and I. Chakraborty, *et al.*, The role of ligands in the chemical synthesis and applications of inorganic nanoparticles, *Chem. Rev.*, 2019, **119**(8), 4819–4880.

25 J. Il Park, A. Saffari, S. Kumar, A. Günther and E. Kumacheva, Microfluidic, Synthesis of Polymer and Inorganic Particulate Materials, *Annu. Rev. Mater. Res.*, 2010, **40**(1), 415–443.

26 G. Tofighi, H. Lichtenberg, J. Pesek, T. L. Sheppard, W. Wang and L. Schöttner, *et al.*, Continuous microfluidic synthesis of colloidal ultrasmall gold nanoparticles: in situ study of the early reaction stages and application for catalysis, *React. Chem. Eng.*, 2017, **2**, 876–884.

27 L. Wang, S. Ma, B. Yang, W. Cao and X. Han, Morphology-controlled synthesis of Ag nanoparticle decorated poly(o-phenylenediamine) using microfluidics and its application for hydrogen peroxide detection, *Chem. Eng. J.*, 2015, **268**, 102–108.

28 H. Yagyu, Y. Tanabe, S. Takano and M. Hamamoto, Continuous flow synthesis of monodisperse gold nanoparticles by liquid-phase reduction method on glass microfluidic device, *Micro Nano Lett.*, 2017, **12**(8), 536–539.

29 M. Jiao, J. Zeng, L. Jing, C. Liu and M. Gao, Flow synthesis of biocompatible Fe3O4nanoparticles: Insight into the effects of residence time, fluid velocity, and tube reactor dimension on particle size distribution, *Chem. Mater.*, 2015, **27**(4), 1299–1305.

30 S. E. Lohse, J. R. Eller, S. T. Sivapalan, M. R. Plews and C. J. Murphy, A simple millifluidic benchtop reactor system for the high-throughput synthesis and functionalization of gold nanoparticles with different sizes and shapes, *ACS Nano*, 2013, **7**(5), 4135–4150.

31 H. Jun, T. Fabienne, M. Florent, P. E. Coulon, M. Nicolas and S. Olivier, Understanding of the size control of biocompatible gold nanoparticles in millifluidic channels, *Langmuir*, 2012, **28**(45), 15966–15974.

32 J. Polte, R. Erler, A. F. Thünemann, S. Sokolov, T. T. Ahner and K. Rademann, *et al.*, Nucleation and Growth of Gold, *ACS Nano*, 2010, **4**(2), 1076–1082.

33 L. Xu, C. Srinivasakannan, J. Peng, M. Yan, D. Zhang and L. Zhang, Microfluidic reactor synthesis and photocatalytic behavior of Cu@Cu2O nanocomposite, *Appl. Surf. Sci.*, 2015, **331**, 449–454.

34 L. Xu, C. Srinivasakannan, J. Peng, L. Zhang and D. Zhang, Synthesis of Cu-CuO nanocomposite in microreactor and its application to photocatalytic degradation, *J. Alloys Compd.*, 2017, **695**, 263–269.

35 N. Hayashi, Y. Sakai, H. Tsunoyama and A. Nakajima, Development of ultrafine multichannel microfluidic mixer for synthesis of bimetallic nanoclusters: Catalytic application of highly monodisperse AuPd nanoclusters stabilized by poly(N -vinylpyrrolidone), *Langmuir*, 2014, **30**(34), 10539–10547.

36 R. Baber, L. Mazzei, N. T. K. Thanh and A. Gavriilidis, Synthesis of silver nanoparticles in a microfluidic coaxial flow reactor, *RSC Adv.*, 2015, **5**(116), 95585–95591.

37 A. Abou-Hassan, S. Neveu, V. Dupuis and V. Cabuil, Synthesis of cobalt ferrite nanoparticles in continuous-flow microreactors, *RSC Adv.*, 2012, **2**(30), 11263–11266.

38 K. N. Han, C. A. Li, M. P. N. Bui, X. H. Pham, B. S. Kim and Y. H. Choa, *et al.*, On-chip electrochemical detection of bio/chemical molecule by nanostructures fabricated in a microfluidic channel, *Sens. Actuators, B*, 2013, **177**, 472–477.

39 L. Hafermann and J. M. Köhler, Photochemical Micro Continuous-Flow Synthesis of Noble Metal Nanoparticles of the Platinum Group, *Chem. Eng. Technol.*, 2015, **38**(7), 1138–1143.

40 T. Ishizaka, A. Ishigaki, H. Kawanami, A. Suzuki and T. M. Suzuki, Dynamic control of gold nanoparticle morphology in a microchannel flow reactor by glucose reduction in aqueous sodium hydroxide solution, *J. Colloid Interface Sci.*, 2012, **367**(1), 135–138.

41 D. H. Napper, Colloid Stability, *Ind. Eng. Chem. Prod. Res. Dev.*, 1970, **9**(4), 467–477.

42 D. H. Napper, Steric stabilization, *J. Colloid Interface Sci.*, 1977, **58**(2), 390–407.
43 T. A. Witten, P. A. Pincus and P. A. Pincus, Colloid Stabilization by Long Grafted Polymers, *Macromolecules*, 1986, **19**(10), 2509–2513.
44 H. Hu, J. H. Xin, H. Hu, X. Wang, D. Miao and Y. Liu, Synthesis and stabilization of metal nanocatalysts for reduction reactions - A review, *J. Mater. Chem. A*, 2015, **3**(21), 11157–11182.
45 J. A. Lopez-Sanchez, N. Dimitratos, C. Hammond, G. L. Brett, L. Kesavan and S. White, *et al.*, Facile removal of stabilizer-ligands from supported gold nanoparticles, *Nat. Chem.*, 2011, **3**(7), 551–556.
46 M.-C. Daniel and D. Astruc, Gold Nanoparticles: Assembly, Supramolecular Chemistry, Quantum-Size-Related Properties, and Applications toward Biology, Catalysis, and Nanotechnology, *Chem. Rev.*, 2004, **104**(1), 293–346.
47 P. J. Kitson, M. H. Rosnes, V. Sans, V. Dragone and L. Cronin, Configurable 3D-Printed millifluidic and microfluidic "lab on a chip" reactionware devices, *Lab Chip*, 2012, **12**, 3267–3271.
48 G. Tofighi, H. Lichtenberg, J. Pesek, T. L. Sheppard, W. Wang and L. Schöttner, *et al.*, Continuous microfluidic synthesis of colloidal ultrasmall gold nanoparticles: in situ study of the early reaction stages and application for catalysis, *React. Chem. Eng.*, 2017, **2**, 876–884.
49 M. V. Bandulasena, G. T. Vladisavljević, O. G. Odunmbaku and B. Benyahia, Continuous synthesis of PVP stabilized biocompatible gold nanoparticles with a controlled size using a 3D glass capillary microfluidic device, *Chem. Eng. Sci.*, 2017, **171**, 233–243.
50 L. Uson, V. Sebastian, M. Arruebo and J. Santamaria, Continuous microfluidic synthesis and functionalization of gold nanorods, *Chem. Eng. J.*, 2016, **285**, 286–292.
51 Q. Fu, Y. Sheng, H. Tang, Z. Zhu, M. Ruan and W. Xu, *et al.*, Growth Mechanism Deconvolution of Self- Growth Mechanism Deconvolution of Self-Limiting Supraparticles Based on Micro fl uidic System, *ACS Nano*, 2015, **9**(1), 172–179.
52 L. Gomez, V. Sebastian, S. Irusta, A. Ibarra, M. Arruebo and J. Santamaria, Scaled-up production of plasmonic nanoparticles using microfluidics: from metal precursors to functionalized and sterilized nanoparticles, *Lab Chip*, 2014, **14**(2), 325–332.
53 K. Sai Krishna, C. V. Navin, S. Biswas, V. Singh, K. Ham and G. L. Bovenkamp, *et al.*, Millifluidics for time-resolved mapping of the growth of gold nanostructures, *J. Am. Chem. Soc.*, 2013, **135**(14), 5450–5456.
54 A. Sugie, H. Song, T. Horie, N. Ohmura, K. Kanie and A. Muramatsu, *et al.*, Synthesis of thiol-capped gold nanoparticle with a flow system using organosilane as a reducing agent, *Tetrahedron Lett.*, 2012, **53**(33), 4457–4459.
55 M. Luty-Błocho, K. Fitzner, V. Hessel, P. Löb, M. Maskos and D. Metzke, *et al.*, Synthesis of gold nanoparticles in an interdigital micromixer using ascorbic acid and sodium borohydride as reducers, *Chem. Eng. J.*, 2011, **171**(1), 279–290.
56 K. Sugano, Y. Uchida, O. Ichihashi, H. Yamada, T. Tsuchiya and O. Tabata, Mixing speed-controlled gold nanoparticle synthesis with pulsed mixing microfluidic system, *Microfluid. Nanofluid.*, 2010, **9**(6), 1165–1174.
57 J. Polte, R. Erler, A. F. Thünemann, S. Sokolov, T. T. Ahner and K. Rademann, *et al.*, Nucleation and Growth of Gold Nanoparticles Studied via in situ Small Angle X-ray Scattering at Millisecond Time Resolution, *ACS Nano*, 2010, **4**(2), 1076–1082.
58 S. G. Pedro, M. Puyol, D. Izquierdo, Í. Salinas and J. Alonso, Group B, *et al.*, *Synthesis of MUA-protected gold nanoparticles in microfluidic devices with in situ UV-vis characterization. Conf Ibersensor November*, Lisbon, 2010.
59 C. Bullen, M. J. Latter, N. J. D'Alonzo, G. J. Willis and C. L. Raston, A seedless approach to continuous flow synthesis of gold nanorods, *Chem. Commun.*, 2011, **47**(14), 4123–4125.
60 S. Horikoshi, T. Sumi and N. Serpone, A Hybrid Microreactor/Microwave High-Pressure Flow System of a Novel Concept Design and its Application to the Synthesis of Silver Nanoparticles, *Chem. Eng. Process.*, 2013, **73**, 59–66.
61 H. Liu, J. Huang, D. Sun, L. Lin, W. Lin and J. Li, *et al.*, Microfluidic biosynthesis of silver nanoparticles: Effect of process parameters on size distribution, *Chem. Eng. J.*, 2012, **209**, 568–576.
62 A. M. Karim, N. Al Hasan, S. Ivanov, S. Siefert, R. T. Kelly and N. G. Hallfors, *et al.* Synthesis of 1 nm Pd Nanoparticles in a Microfluidic Reactor: Insights from in Situ X-ray Absorption Fine Structure Spectroscopy and Small-Angle X-ray Scattering, *J. Phys. Chem. C*, 2015, **119**(23), 13257–13267.
63 H. Liang, Z. Wang, J. Wang, D. Huang, Y. Zhu and Y. Song, Synthesis of Fe(1-x)Znx@Zn(1-y)FeyOz nanocrystals via a simple programmed microfluidic process, *Mater. Chem. Phys.*, 2017, **201**, 156–164.
64 Y. Song, R. Li, Q. Sun and P. Jin, Controlled growth of Cu nanoparticles by a tubular microfluidic reactor, *Chem. Eng. J.*, 2011, **168**(1), 477–484.
65 L. Xu, C. Srinivasakannan, J. Peng, D. Zhang and G. Chen, Synthesis of nickel nanoparticles by aqueous reduction in continuous flow microreactor, *Chem. Eng. Process.*, 2015, **93**, 44–49.
66 R. Eluri and B. Paul, Synthesis of nickel nanoparticles by hydrazine reduction: Mechanistic study and continuous flow synthesis, *J. Nanopart. Res.*, 2012, **14**(4), 1–14.
67 P. L. Suryawanshi, S. P. Gumfekar, P. R. Kumar, B. B. Kale and S. H. Sonawane, Synthesis of ultra-small platinum nanoparticles in a continuous flow microreactor, *Colloid Interface Sci. Commun.*, 2016, **13**, 6–9.
68 M. J. Hossain, H. Tsunoyama, M. Yamauchi, N. Ichikuni and T. Tsukuda, High-yield synthesis of PVP-stabilized small Pt clusters by microfluidic method, *Catal. Today*, 2012, **183**(1), 101–107.
69 S. Abalde-Cela, P. Taladriz-Blanco, M. G. De Oliveira and C. Abell, Droplet microfluidics for the highly controlled

synthesis of branched gold nanoparticles, *Sci. Rep.*, 2018, **8**, 2440–2446.

70 L. L. Lazarus, C. T. Riche, B. C. Marin, M. Gupta, N. Malmstadt and R. L. Brutchey, Two-phase microfluidic droplet flows of ionic liquids for the synthesis of gold and silver nanoparticles, *ACS Appl. Mater. Interfaces*, 2012, **4**(6), 3077–3083.

71 L. L. Lazarus, A. S.-J. Yang, S. Chu, R. L. Brutchey and N. Malmstadt, Flow-focused synthesis of monodisperse gold nanoparticles using ionic liquids on a microfluidic platform, *Lab Chip*, 2010, **10**(24), 3377–3379.

72 L. Xu, J. Peng, C. Srinivasakannan, L. Zhang, D. Zhang and C. Liu, *et al.*, Synthesis of copper nanoparticles by a T-shaped microfluidic device, *RSC Adv.*, 2014, **4**(48), 25155–25159.

73 L. Zhang, Y. Wang, L. Tong and Y. Xia, Seed-mediated synthesis of silver nanocrystals with controlled sizes and shapes in droplet microreactors separated by air, *Langmuir*, 2013, **29**(50), 15719–15725.

74 L. Hafermann and K. J. Michael, Small gold nanoparticles formed by rapid photochemical flow-through synthesis using microfluid segment technique, *J. Nanopart. Res.*, 2015, **17**(2), 1–8.

75 Y. H. Kim, L. Zhang, T. Yu, M. Jin, D. Qin and Y. Xia, Droplet-based microreactors for continuous production of palladium nanocrystals with controlled sizes and shapes, *Small*, 2013, **9**, 3462–3467.

76 K. Kumar, A. M. Nightingale, S. H. Krishnadasan, N. Kamaly, M. Wylenzinska-Arridge and K. Zeissler, *et al.*, Direct synthesis of dextran-coated superparamagnetic iron oxide nanoparticles in a capillary-based droplet reactor, *J. Mater. Chem.*, 2012, **22**(11), 4704–4708.

77 K. G. Lee, J. Hong, K. W. Wang, N. S. Heo, D. H. Kim and S. Y. Lee, *et al.*, In VitroBiosynthesis of Metal Nanoparticles in Microdroplets, *ACS Nano*, 2012, **6**(8), 6998–7008.

78 L. Zhang, G. Niu, N. Lu, J. Wang, L. Tong and L. Wang, *et al.*, Continuous and scalable production of well-controlled noble-metal nanocrystals in milliliter-sized droplet reactors, *Nano Lett.*, 2014, **14**(11), 6626–6631.

79 X. Li, N. Visaveliya, L. Hafermann, G. A. Gross, A. Knauer and J. M. Köhler, Hierarchically structured particles for micro flow catalysis, *Chem. Eng. J.*, 2017, **326**, 1058–1065.

80 D. V. Ravi Kumar, B. L. V. Prasad and A. A. Kulkarni, Segmented flow synthesis of Ag nanoparticles in spiral microreactor: Role of continuous and dispersed phase, *Chem. Eng. J.*, 2012, **192**, 357–368.

81 V. Sebastian Cabeza, S. Kuhn, A. A. Kulkarni and K. F. Jensen, Size-Controlled Flow Synthesis of Gold Nanoparticles Using a Segmented Flow Micro fluidic Platform, *Langmuir*, 2012, **28**(17), 7007–7013.

82 D. Zhang, F. Wu, M. Peng, X. Wang, D. Xia and G. Guo, One-step, facile and ultrafast synthesis of phase- and size-controlled Pt-Bi intermetallic nanocatalysts through continuous-flow microfluidics, *J. Am. Chem. Soc.*, 2015, **137**(19), 6263–6269.

83 Z. Wang, H. Fan, H. Liang, J. Ma, S. Li and Y. Song, *et al.*, Microfluidic Synthesis and Characterization of FePtSn/C Catalysts with Enhanced Electro-Catalytic Performance for Direct Methanol Fuel Cells, *Electrochim. Acta*, 2017, **230**, 245–254.

84 S. Tao, M. Yang, H. Chen, M. Ren and G. Chen, Microfluidic synthesis of Ag@Cu2O core-shell nanoparticles with enhanced photocatalytic activity, *J. Colloid Interface Sci.*, 2017, **486**, 16–26.

85 Z. H. Tian, Y. J. Wang, J. H. Xu and G. S. Luo, Intensification of nucleation stage for synthesizing high quality CdSe quantum dots by using preheated precursors in microfluidic devices, *Chem. Eng. J.*, 2016, **302**, 498–502.

86 Z. H. Tian, J. H. Xu, Y. J. Wang and G. S. Luo, Microfluidic synthesis of monodispersed CdSe quantum dots nanocrystals by using mixed fatty amines as ligands, *Chem. Eng. J.*, 2016, **285**, 20–26.

87 B. Swain, M. H. Hong, L. Kang, B. S. Kim, N. H. Kim and C. G. Lee, Optimization of CdSe nanocrystals synthesis with a microfluidic reactor and development of combinatorial synthesis process for industrial production, *Chem. Eng. J.*, 2017, **308**, 311–321.

88 J. Wang, H. Zhao, Y. Zhu and Y. Song, Shape-Controlled Synthesis of CdSe Nanocrystals via a Programmed Microfluidic Process, *J. Phys. Chem. C*, 2017, **121**(6), 3567–3572.

89 I. Lignos, S. Stavrakis, A. Kilaj and A. J. deMello, Millisecond-Timescale Monitoring of PbS Nanoparticle Nucleation and Growth Using Droplet-Based Microfluidics, *Small*, 2015, **11**(32), 4009–4017.

90 N. J. Carroll, P. F. Crowder, S. Pylypenko, W. Patterson, D. R. Ratnaweera and D. Perahia, *et al.*, Microfluidic synthesis of monodisperse nanoporous oxide particles and control of hierarchical pore structure, *ACS Appl. Mater. Interfaces*, 2013, **5**(9), 3524–3529.

91 N. Bchellaoui, Z. Hayat, M. Mami, R. Dorbez-Sridi and A. I. El Abed, Microfluidic-assisted Formation of Highly Monodisperse and Mesoporous Silica Soft Microcapsules, *Sci. Rep.*, 2017, **7**, 1–10.

92 Y. Nie, N. Hao and J. X. J. Zhang, Ultrafast Synthesis of Multifunctional Submicrometer Hollow Silica Spheres in Microfluidic Spiral Channels, *Sci. Rep.*, 2017, **7**(1), 1–9.

93 I. Lee, Y. Yoo, Z. Cheng and H. K. Jeong, Generation of monodisperse mesoporous silica microspheres with controllable size and surface morphology in a microfluidic device, *Adv. Funct. Mater.*, 2008, **18**(24), 4014–4021.

94 L. Yu, Y. Pan, C. Wang and L. Zhang, A two-phase segmented microfluidic technique for one-step continuous versatile preparation of zeolites, *Chem. Eng. J.*, 2013, **219**, 78–85.

95 J. Ju, C. Zeng, L. Zhang and N. Xu, Continuous synthesis of zeolite NaA in a microchannel reactor, *Chem. Eng. J.*, 2006, **116**(2), 115–121.

96 Y. Pan, J. Yao, L. Zhang and N. Xu, Preparation of Ultrafine Zeolite A Crystals with Narrow Particle Size Distribution Using a Two-Phase Liquid Segmented Microfluidic Reactor, *Ind. Eng. Chem. Res.*, 2009, **48**(18), 8471–8477.

97 P. H. Hoang, K. B. Yoon and D. P. Kim, Synthesis of hierarchically porous zeolite A crystals with uniform

particle size in a droplet microreactor, *RSC Adv.*, 2012, **2**(12), 5323–5328.

98 M. Faustini, J. Kim, G. Jeong, J. Y. Kim, H. R. Moon and W. Ahn, *et al.*, Microfluidic Approach toward Continuous and Ultrafast Synthesis of Metal – Organic Framework Crystals and Hetero Structures in Confined Microdroplets, *J. Am. Chem. Soc.*, 2013, **135**, 14619–14626.

99 D. Witters, N. Vergauwe, R. Ameloot, S. Vermeir, D. De Vos, R. Puers, B. Sels and J. Lammertyn, Digital Microfluidic High-Throughput Printing of Single Metal-Organic Framework Crystals, *Adv. Mater.*, 2012, **24**, 1316–1320.

100 J. D. Tice, H. Song, A. D. Lyon and R. F. Ismagilov, Formation of Droplets and Mixing in Multiphase Microfluidics at Low Values of the Reynolds and the Capillary Numbers, *Langmuir*, 2003, **19**(22), 9127–9133.

101 R. O. Grigoriev, M. F. Schatz and V. Sharma, Chaotic mixing in microdroplets, *Lab Chip*, 2006, **6**(10), 1369.

102 A. M. Nightingale and J. C. De Mello, Microscale synthesis of quantum dots, *J. Mater. Chem.*, 2010, **20**(39), 8454–8463.

103 J. Baek, Y. Shen, I. Lignos, M. G. Bawendi and K. F. Jensen, Multistage Microfluidic Platform for the Continuous Synthesis of III–V Core/Shell Quantum Dots, *Angew. Chem., Int. Ed.*, 2018, **57**(34), 10915–10918.

104 J. D. Rimer, M. Kumar, R. Li, A. I. Lupulescu and M. D. Oleksiak, Tailoring the physicochemical properties of zeolite catalysts, *Catal. Sci. Technol.*, 2014, **4**(11), 3762–3771.

105 Y. Pan, J. Yao, L. Zhang, J. Ju, H. Wang and N. Xu, Rapid crystallization of silicalite nanocrystals in a capillary microreactor, *Chem. Eng. Technol.*, 2009, **32**(5), 732–737.

106 A. Dhakshinamoorthy, L. Zhaohui and H. Garcia, Catalysis and photocatalysis by metal organic framewoks, *Chem. Soc. Rev.*, 2018, **47**, 8134–8172.

107 Y. Song, D. Cheng, L. Zhao, F. Cacho-Bailo, C. Téllez and J. Coronas, Microfluidic Synthesis of MOFs and MOF-Based Membranes, *Microfluid Fundam Devices Appl.*, 2018, pp. 479–515.

108 S. Zhao, Y. Li, E. Stavitski, R. Tappero, S. Crowley and M. J. Castaldi, *et al.*, Operando Characterization of Catalysts through use of a Portable Microreactor, *ChemCatChem*, 2015, **7**(22), 3683–3691.

109 Q. Zhang, Q. Zhang, H. Wang and Y. Li, A high efficiency microreactor with Pt/ZnO nanorod arrays on the inner wall for photodegradation of phenol, *J. Hazard. Mater.*, 2013, **254–255**(1), 318–324.

110 Z. He, Y. Li, Q. Zhang and H. Wang, Capillary microchannel-based microreactors with highly durable ZnO/TiO2nanorod arrays for rapid, high efficiency and continuous-flow photocatalysis, *Appl. Catal., A*, 2010, **93**(3–4), 376–382.

111 S. Hannemann, J. D. Grunwaldt, N. van Vegten, A. Baiker, P. Boye and C. G. Schroer, Distinct spatial changes of the catalyst structure inside a fixed-bed microreactor during the partial oxidation of methane over Rh/Al2O3, *Catal. Today*, 2007, **126**(1–2), 54–63.

112 L.-S. Bouchard, S. R. Burt, M. S. Anwar, K. V. Kovtunov, I. V. Koptyung and A. Pines, NMR Imaging of Catalytic Hydrogenation in Microreactors with the Use of para-Hydrogen, *Science*, 2008, **319**, 442–445.

113 H. Zhang, J. J. Wang, J. Fan and Q. Fang, Microfluidic chip-based analytical system for rapid screening of photocatalysts, *Talanta*, 2013, **116**, 946–950.

114 A. L. Liu, Z. Q. Li, Z. Q. Wu and X. H. Xia, Study on the photocatalytic reaction kinetics in a TiO2nanoparticles coated microreactor integrated microfluidics device, *Talanta*, 2018, **182**, 544–548.

115 J. Gmeiner, S. Behrens, B. Spliethoff and O. Trapp, Ruthenium Nanoparticles in High-Throughput Studies of Chemoselective Carbonyl Hydrogenation Reactions, *ChemCatChem*, 2016, **8**(3), 571–576.

116 E. Gross, X. Z. Shu, S. Alayoglu, H. A. Bechtel, M. C. Martin and F. D. Toste, *et al.*, In situ IR and X-ray high spatial-resolution microspectroscopy measurements of multistep organic transformation in flow microreactor catalyzed by Au nanoclusters, *J. Am. Chem. Soc.*, 2014, **136**(9), 3624–3629.

117 Z. Zhang, U. Gernert, R. F. Gerhardt, E. M. Höhn, D. Belder and J. Kneipp, Catalysis by Metal Nanoparticles in a Plug-In Optofluidic Platform: Redox Reactions of p-Nitrobenzenethiol and p-Aminothiophenol, *ACS Catal.*, 2018, **8**(3), 2443–2449.

118 X. Z. Lin, A. D. Terepka and H. Yang, Synthesis of silver nanoparticles in a continuous flow tubular microreactor, *Nano Lett.*, 2004, **4**(11), 2227–2232.

119 S. Biswas, J. T. Miller, Y. Li, K. Nandakumar and C. S. S. R. Kumar, Developing a millifluidic platform for the synthesis of ultrasmall nanoclusters: Ultrasmall copper nanoclusters as a case study, *Small*, 2012, **8**(5), 688–698.

120 C. V. Navin, K. S. Krishna, G. L. Bovenkamp-Langlois, J. T. Miller, S. Chattopadhyay and T. Shibata, *et al.*, Investigation of the synthesis and characterization of platinum-DMSA nanoparticles using millifluidic chip reactor, *Chem. Eng. J.*, 2015, **281**, 81–86.

121 G. Sankar, E. Cao and A. Gavriilidis, A microstructured reactor based in situ cell for the study of catalysts by X-ray absorption spectroscopy under operating conditions, *Catal. Today*, 2007, **125**(1–2), 24–28.

122 J. Yue, J. C. Schouten and N. T. Alexander, Integration of microreactors with spectroscopic detection for online reaction monitoring and catalyst characterization, *Ind. Eng. Chem. Res.*, 2012, **51**(45), 14583–14609.

123 A. V. Pattekar and M. V. Kothare, A microreactor for hydrogen production in micro fuel cell applications, *J. Microelectromech. Syst.*, 2004, **13**(1), 7–18.

124 H. Li, X. Yu, S. T. Tu, J. Yan and Z. Wang, Catalytic performance and characterization of Al2O 3-supported Pt-Co catalyst coatings for preferential CO oxidation in a micro-reactor, *Appl. Catal., A*, 2010, **387**(1–2), 215–223.

125 T. R. Henriksen, J. L. Olsen, P. Vesborg, I. Chorkendorff and O. Hansen, Highly sensitive silicon microreactor for catalyst testing, *Rev. Sci. Instrum.*, 2009, **80**(12), 124101.

126 P. Kondratyuk, G. Gumuslu, S. Shukla, J. B. Miller, B. D. Morreale and A. J. Gellman, A microreactor array for

spatially resolved measurement of catalytic activity for high-throughput catalysis science, *J. Catal.*, 2013, **300**, 55–62.

127 S. K. Ajmera, C. Delattre, M. A. Schmidt and K. F. Jensen, Microfabricated differential reactor for heterogeneous gas phase catalyst testing, *J. Catal.*, 2002, **209**(2), 401–412.

128 S. K. Ajmera, C. Delattre, M. A. Schmidt, K. F. Jensen, Microreactors for measuring catalyst activity and determining reaction kinetics, *Science and Technology in Catalysis 2002*, 2003, vol. 145 pp. 97–102.

129 S. Hannemann, J. D. Grunwaldt, B. Kimmerle, A. Baiker, P. Boye and C. Schroer, Axial changes of catalyst structure and temperature in a fixed-bed microreactor during noble metal catalysed partial oxidation of methane, *Top. Catal.*, 2009, **52**(10), 1360–1370.

130 E. Cao, M. Sankar, S. Firth, K. F. Lam, D. Bethell and D. K. Knight, *et al.*, Reaction and Raman spectroscopic studies of alcohol oxidation on gold-palladium catalysts in microstructured reactors, *Chem. Eng. J.*, 2011, **167**(2–3), 734–743.

131 V. V. Zhivonitko, V. V. Telkki and I. V. Koptyug, Characterization of microfluidic gas reactors using remote-detection MRI and parahydrogen-induced polarization, *Angew. Chem., Int. Ed.*, 2012, **51**(32), 8054–8058.

132 K. Olivon and F. Sarrazin, Heterogeneous reaction with solid catalyst in droplet-flow millifluidic device, *Chem. Eng. J.*, 2013, **227**, 97–102.

133 S. Ponce, M. Munoz, A. M. Cubillas, T. G. Euser, G. R. Zhang and P. S. J. Russell, *et al.*, Stable Immobilization of Size-Controlled Bimetallic Nanoparticles in Photonic Crystal Fiber Microreactor, *Chem. Ing. Tech.*, 2018, **90**(5), 653–659.

134 A. Aguirre, P. A. Kler, C. L. A. Berli and S. E. Collins, Design and operational limits of an ATR-FTIR spectroscopic microreactor for investigating reactions at liquid-solid interface, *Chem. Eng. J.*, 2014, **243**, 197–206.

135 W. Xie, R. Grzeschik and S. Schlücker, Metal Nanoparticle-Catalyzed Reduction Using Borohydride in Aqueous Media: A Kinetic Analysis of the Surface Reaction by Microfluidic SERS, *Angew. Chem., Int. Ed.*, 2016, **55**(44), 13729–13733.

136 R. Ricciardi, J. Huskens and W. Verboom, Influence of the Au/Ag ratio on the catalytic activity of dendrimer-encapsulated bimetallic nanoparticles in microreactors, *J Flow Chem.*, 2015, **5**, 228–233.

137 D. C. Harris, Methods in Geochemistry and Geophysics, *Quantitative Chemical Analysis*, 1971, vol. 5, pp. 89–142.

138 Y. Li, B. Lin, L. Ge, H. Guo, X. Chen and M. Lu, Real-time spectroscopic monitoring of photocatalytic activity promoted by graphene in a microfluidic reactor, *Sci. Rep.*, 2016, **6**, 1–9.

139 mempax@www.pgo-online.com.

140 Y. Song, H. Modrow, L. L. Henry, C. K. Saw, E. E. Doomes and V. Palshin, *et al.*, Microfluidic synthesis of cobalt nanoparticles, *Chem. Mater.*, 2006, **18**(12), 2817–2827.

141 C. H. Bartholomew, Mechanism of catalyst deactivation, *Appl. Catal., A*, 2001, **212**, 17–60.

142 E. Karabudak, Micromachined silicon attenuated total reflectance infrared spectroscopy: An emerging detection method in micro/nanofluidics, *Electrophoresis*, 2014, **35**(2–3), 236–244.

143 J. R. Ferraro, K. Nakamoto and C. W. Brown, *Introductory Raman Spectroscopy*, North-Holland Mathematics Studies, 2005, vol. 202, pp. 1–45.

144 S. Schlücker, Surface-enhanced raman spectroscopy: Concepts and chemical applications, *Angew. Chem., Int. Ed.*, 2014, **53**(19), 4756–4795.

145 E. Smith and G. Dent, *A Practical Approach, Modern Raman Spectroscopy*, 2005.

146 F. Meirer, S. Kalirai, J. N. Weker, Y. Liu, J. C. Andrews and B. M. Weckhuysen, Agglutination of single catalyst particles during fluid catalytic cracking as observed by X-ray nanotomography, *Chem. Commun.*, 2015, **51**, 8097–8100.

147 M. Jin, V. Pully, C. Otto, A. Van Den Berg and E. T. Carlen, High-density periodic arrays of self-aligned subwavelength nanopyramids for surface-enhanced Raman spectroscopy, *J. Phys. Chem. C*, 2010, **114**(50), 21953–21959.

148 C. D. Baertsch, M. A. Schmidt and K. F. Jensen, Catalyst surface characterization in microfabricated reactors using pulse chemisorption, *Chem. Commun.*, 2004, 2610–2611.

149 W. Chen, P. Vashistha, A. Yen, N. Joshi, Y. Kapoor and R. L. Hartman, Asphaltenes Dissolution Mechanism Study by in Situ Raman Characterization of a Packed-Bed Microreactor with HZSM-5 Aluminosilicates, *Energy Fuels*, 2018, **32**(12), 12205–12217.

150 S. K. Lee, X. Liu, V. Sebastián Cabeza and K. F. Jensen, Synthesis, assembly and reaction of a nanocatalyst in microfluidic systems: a general platform, *Lab Chip*, 2012, **12**(20), 4080–4084.

151 R. M. Tiggelaar, F. Benito-López, D. C. Hermes, H. Rathgen, R. J. M. Egberink and F. G. Mugele, *et al.*, Fabrication, mechanical testing and application of high-pressure glass microreactor chips, *Chem. Eng. J.*, 2007, **131**(1–3), 163–170.

152 R. M. Tiggelaar, P. Van Male, J. W. Berenschot, J. G. E. Gardeniers, R. E. Oosterbroek and M. H. J. M. De Croon, *et al.*, Fabrication of a high-temperature microreactor with integrated heater and sensor patterns on an ultrathin silicon membrane, *Sens. Actuators, A*, 2005, **119**(1), 196–205.

153 L. A. Truter, V. Ordomsky, J. C. Schouten and T. A. Nijhuis, The application of palladium and zeolite incorporated chip-based microreactors, *Appl. Catal., A*, 2016, **515**, 72–82.

154 N. C. Pérez, E. E. Miró and J. M. Zamaro, Microreactors based on CuO-CeO2/zeolite films synthesized onto brass microgrids for the oxidation of CO, *Appl. Catal., B*, 2013, **129**, 416–425.

155 R. Dai, Z. Zheng, C. Sun, X. Li, S. Wang and X. Wu, *et al.*, Pt nanoparticles encapsulated in a hollow zeolite microreactor as a highly active and stable catalyst for low-temperature ethanol steam reforming, *Fuel*, 2018, **214**, 88–97.

156 K. He, W. Han and K. L. Yeung, Preparation and performance of catalytic MOFs in microreactor, *J. Taiwan Inst. Chem. Eng.*, 2019, **98**, 85–93.

157 M. Mar Darder, S. Salehinia, J. B. Parra, J. M. Herrero-Martinez, F. Svec and V. Cerda, *et al.*, Nanoparticle-directed metal–organic framework/porous organic polymer monolithic supports for flow-based applications, *ACS Appl. Mater. Interfaces*, 2017, **9**(2), 1728–1736.

158 L. A. Truter, J. Juan-Alcañiz, F. Kapteijn, T. A. Nijhuis, J. Gascon and J. C. Schouten, Metal-Organic Framework Capillary Microreactor for Application in Click Chemistry, *ChemCatChem*, 2016, **8**(9), 1692–1698.

159 Y. Su, S. Li, D. He, D. Yu, F. Liu and N. Shao, *et al.*, MOF-Derived Porous ZnO Nanocages/rGO/Carbon Sponge-Based Photocatalytic Microreactor for Efficient Degradation of Water Pollutants and Hydrogen Evolution, *ACS Sustainable Chem. Eng.*, 2018, **6**(9), 11989–11998.

160 I. L. C. Buurmans, J. Ruiz-martínez, W. V. Knowles, D. Van Der Beek, J. A. Bergwerff and E. T. C. Vogt, *et al.*, Catalytic activity in individual cracking catalyst particles imaged throughout different life stages by selective staining, *Nat. Chem.*, 2011, **3**, 862–867.

161 G. Morra, A. Desmartin-Chomel, C. Daniel, U. Ravon, D. Farrusseng and R. Cowan, *et al.*, High-throughput gas phase transient reactor for catalytic material characterization and kinetic studies, *Chem. Eng. J.*, 2008, **138**(1–3), 379–388.

162 D. T. D. Childs, R. A. Hogg, D. G. Revin, I. U. Rehman, J. W. Cockburn and S. J. Matcher, Sensitivity Advantage of QCL Tunable-Laser Mid-Infrared Spectroscopy over FTIR Spectroscopy, *Appl. Spectrosc. Rev.*, 2015, **50**(10), 822–839.

163 W. Schlindwein, M. Bezerra, J. Almeida, A. Berghaus, M. Owen and G. Muirhead, In-line uv-vis spectroscopy as a fast-working process analytical technology (Pat) during early phase product development using hot melt extrusion (hme), *Pharmaceutics*, 2018, **10**(4), 1–25.

164 Y. Kumamoto, Y. Harada, T. Takamatsu and H. Tanaka, Label-free Molecular Imaging and Analysis by Raman Spectroscopy, *Acta Histochem. Cytochem.*, 2018, **51**(3), 101–110.

165 Real-Time Gas Analysis and Reaction Monitoring using Mass Spectrometry, Available from: https://www.hidenanalytical.com/real-time-gas-analysis-reaction-monitoring-using-mass-spectrometry/.

166 E. Seres and C. Spielmann, Ultrafast soft x-ray absorption spectroscopy with sub- 20-fs resolution, *Appl. Phys. Lett.*, 2007, **91**(12), 89–92.

167 O. Müller, M. Nachtegaal, J. Just, D. Lützenkirchen-Hecht and R. Frahm, Quick-EXAFS setup at the SuperXAS beamline for in situ X-ray absorption spectroscopy with 10ms time resolution, *J. Synchrotron Radiat.*, 2016, **23**, 260–266.

168 A. G. Palmer, NMR Characterization of the Dynamics of Biomacromolecules, *Chem. Rev.*, 2004, **104**(8), 3623–3640.

169 I. L. C. Buurmans and B. M. Weckhuysen, Heterogeneities of individual catalyst particles in space and time as monitored by spectroscopy, *Nat. Chem.*, 2012, **4**(11), 873–886.

170 Y. Liu and X. Jiang, Why microfluidics? Merits and trends in chemical synthesis, *Lab Chip*, 2017, **17**(23), 3960–3978.

171 F. Malloggi, N. Pannacci, R. Attia, F. Monti, P. Mary and H. Willaime, *et al.*, Monodisperse colloids synthesized with nanofluidic technology, *Langmuir*, 2010, **26**(4), 2369–2373.

172 E. Amstad, X. Chen, M. Eggersdorfer, N. Cohen, T. E. Kodger and C. L. Ren, *et al.*, Parallelization of microfluidic flow-focusing devices, *Phys. Rev. E*, 2017, **95**(4), 43105.

173 M. Leman, F. Abouakil, A. D. Griffiths and P. Tabeling, Droplet-based microfluidics at the femtolitre scale, *Lab Chip*, 2015, **15**(3), 753–765.

174 N. Toshima and T. Yonezawa, Bimetallic nanoparticles—novel materials for chemical and physical applications, *New J. Chem.*, 1998, **22**(11), 1179–1201.

175 D. Ferrer, A. Torres-Castro, X. Gao, S. Sepúlveda-Guzmán, U. Ortiz-Méndez and M. José-Yacamán, Three-layer core/shell structure in Au-Pd bimetallic nanoparticles, *Nano Lett.*, 2007, **7**(6), 1701–1705.

176 J. H. Park, C. M. Han, E. J. Lee and H. W. Kim, Preparation of highly monodispersed porous-channeled poly-(caprolactone) microspheres by a microfluidic system, *Mater. Lett.*, 2016, **181**, 92–98.

177 I. K. Sung, Christian, M. Mitchell, D. P. Kim and P. J. A. Kenis, Tailored macroporous SiCN and SiC structures for high-temperature fuel reforming, *Adv. Funct. Mater.*, 2005, **15**(8), 1336–1342.

178 B. De Nijs, S. Dussi, F. Smallenburg, J. D. Meeldijk, D. J. Groenendijk and L. Filion, *et al.*, Entropy-driven formation of large icosahedral colloidal clusters by spherical confinement, *Nat. Mater.*, 2015, **14**(1), 56–60.

179 M. N. Lee and A. Mohraz, Bicontinuous macroporous materials from bijel templates, *Adv. Mater.*, 2010, **22**(43), 4836–4841.

180 M. F. Haase, K. J. Stebe and D. Lee, Continuous Fabrication of Hierarchical and Asymmetric Bijel Microparticles, Fibers, and Membranes by Solvent Transfer-Induced Phase Separation (STRIPS), *Adv. Mater.*, 2015, **27**(44), 7065–7071.

181 E. Amstad, F. Spaepen, M. P. Brenner and D. A. Weitz, The microfluidic nebulator: production of sub-micrometer sized airborne drops, *Lab Chip*, 2017, **17**(8), 1475–1480.

182 S. Yadavali, H. H. Jeong, D. Lee and D. Issadore, Silicon and glass very large scale microfluidic droplet integration for terascale generation of polymer microparticles, *Nat. Commun.*, 2018, **9**(1), 1222.

183 E. Amstad, M. Chemama, M. Eggersdorfer, L. R. Arriaga, M. P. Brenner and D. A. Weitz, Robust scalable high throughput production of monodisperse drops, *Lab Chip*, 2016, **16**(21), 4163–4172.

184 A. Ofner, D. G. Moore, P. A. Rühs, P. Schwendimann, M. Eggersdorfer and E. Amstad, *et al.*, High-Throughput Step Emulsification for the Production of Functional Materials Using a Glass Microfluidic Device, *Macromol. Chem. Phys.*, 2017, **218**(2), 1600472.

185 X. Xu, H. Yuan, R. Song, M. Yu, H. Y. Chung and Y. Hou, *et al.*, High aspect ratio induced spontaneous generation of monodisperse picolitre droplets for digital PCR, *Biomicrofluidics*, 2018, **12**(1), 14103.

186 H. Yin and D. Marshall, Microfluidics for single cell analysis, *Curr. Opin. Biotechnol.*, 2012, **23**(1), 110–119.
187 R. Seemann, M. Brinkmann, T. Pfohl and S. Herminghaus, Droplet based microfluidics, *Rep. Prog. Phys.*, 2012, **75**(1), 16601.
188 S. Mashaghi, A. Abbaspourrad, D. A. Weitz and A. M. van Oijen, Droplet microfluidics: A tool for biology, chemistry and nanotechnology, *TrAC, Trends Anal. Chem.*, 2016, **82**, 118–125.
189 J. Krüger, K. Singh, A. O'Neill, C. Jackson, A. Morrison and P. O'Brein, Development of a microfluidic device for fluorescence activated cell sorting, *J. Micromech. Microeng.*, 2002, **12**(4), 486–494.
190 V. Studer, R. Jameson, E. Pellereau, A. Pépin and Y. Chen, A microfluidic mammalian cell sorter based on fluorescence detection, *Microelectron. Eng.*, 2004, **73–74**, 852–857.
191 J. C. Baret, O. J. Miller, V. Taly, M. Ryckelynck, A. El-Harrak and L. Frenz, *et al.*, Fluorescence-activated droplet sorting (FADS): Efficient microfluidic cell sorting based on enzymatic activity, *Lab Chip*, 2009, **9**(13), 1850–1858.
192 E. Brouzes, M. Medkova, N. Savenelli, D. Marran, M. Twardowski and J. B. Hutchison, *et al.*, Droplet microfluidic technology for single-cell high-throughput screening, *Proc. Natl. Acad. Sci. U. S. A.*, 2009, **106**(34), 14195–14200.
193 L. Mazutis, J. C. Baret and A. D. Griffiths, A fast and efficient microfluidic system for highly selective one-to-one droplet fusion, *Lab Chip*, 2009, **9**(18), 2665–2672.
194 A. R. Abate, J. J. Agresti and D. A. Weitz, Microfluidic sorting with high-speed single-layer membrane valves, *Appl. Phys. Lett.*, 2010, **96**(20), 203509.
195 T. H. Wu, Y. Chen, S. Y. Park, J. Hong, T. Teslaa and J. F. Zhong, *et al.*, Pulsed laser triggered high speed microfluidic fluorescence activated cell sorter, *Lab Chip*, 2012, **12**(7), 1378–1383.
196 L. Mazutis, J. Gilbert, W. L. Ung, D. A. Weitz, A. D. Griffiths and J. A. Heyman, Single-cell analysis and sorting using droplet-based microfluidics, *Nat. Protoc.*, 2013, **8**(5), 870–891.
197 P. Hammar, S. A. Angermayr, S. L. Sjostrom, J. Van Der Meer, K. J. Hellingwerf and E. P. Hudson, *et al.*, Single-cell screening of photosynthetic growth and lactate production by cyanobacteria, *Biotechnol. Biofuels*, 2015, **8**(1), 1–8.
198 S. L. Sjostrom, H. N. Joensson and H. A. Svahn, Multiplex analysis of enzyme kinetics and inhibition by droplet microfluidics using picoinjectors, *Lab Chip*, 2013, **13**(9), 1754–1761.
199 E. W. M. Kemna, L. I. Segerink, F. Wolbers, I. Vermes and A. Van Den Berg, Label-free, high-throughput, electrical detection of cells in droplets, *Analyst*, 2013, **138**(16), 4585–4592.
200 K. Ahn, C. Kerbage, T. P. Hunt, R. M. Westervelt, D. R. Link and D. A. Weitz, Dielectrophoretic manipulation of drops for high-speed microfluidic sorting devices, *Appl. Phys. Lett.*, 2006, **88**(2), 1–3.
201 C. W. Lai, Y. H. Lin and G. B. Lee, A microfluidic chip for formation and collection of emulsion droplets utilizing active pneumatic micro-choppers and micro-switches, *Biomed. Microdevices*, 2008, **10**(5), 749–756.
202 C. N. Baroud, J. P. Delville, F. Gallaire and R. Wunenburger, Thermocapillary valve for droplet production and sorting, *Phys. Rev. E: Stat., Nonlinear, Soft Matter Phys.*, 2007, **75**(4), 1–5.
203 M. L. Cordero, D. R. Burnham, C. N. Baroud and D. McGloin, Thermocapillary manipulation of droplets using holographic beam shaping: Microfluidic pin ball, *Appl. Phys. Lett.*, 2008, **93**(3), 2006–2009.
204 T. Franke, A. R. Abate, D. A. Weitz and A. Wixforth, Surface acoustic wave (SAW) directed droplet flow in microfluidics for PDMS devices, *Lab Chip*, 2009, **9**(18), 2625–2627.
205 P. Chen, X. Feng, R. Hu, J. Sun, W. Du and B. F. Liu, Hydrodynamic gating valve for microfluidic fluorescence-activated cell sorting, *Anal. Chim. Acta*, 2010, **663**(1), 1–6.
206 K. Zhang, Q. Liang, S. Ma, X. Mu, P. Hu and Y. Wang, *et al.*, On-chip manipulation of continuous picoliter-volume superparamagnetic droplets using a magnetic force, *Lab Chip*, 2009, **9**(20), 2992–2999.
207 E. Surenjav, C. Priest, S. Herminghaus and R. Seemann, Manipulation of gel emulsions by variable microchannel geometry, *Lab Chip*, 2009, **9**(2), 325–330.
208 M. Solsona, A. E. Nieuwelink, F. Meirer, L. Abelmann, M. Odijk and W. Olthuis, *et al.*, Magnetophoretic Sorting of Single Catalyst Particles, *Angew. Chem., Int. Ed.*, 2018, **57**(33), 10589–10594.
209 M. J. Dejneka, A. Streltsov, S. Pal, A. G. Frutos, C. L. Powell and K. Yost, *et al.*, Rare earth-doped glass microbarcodes, *Proc. Natl. Acad. Sci. U. S. A.*, 2003, **100**(2), 389–393.
210 Y. Fang, N. Yu, Y. Jiang and C. Dang, High-precision lensless flow cytometer on a chip, *Micromachines*, 2018, **9**(5), 1–13.
211 Y. Zhao, H. C. Shum, H. Chen, L. L. A. Adams, Z. Gu and D. A. Weitz, Microfluidic generation of multifunctional quantum dot barcode particles, *J. Am. Chem. Soc.*, 2011, **133**(23), 8790–8793.
212 S. P. Damodaran, S. Eberhard, L. Boitard, J. G. Rodriguez, Y. Wang and N. Bremond, *et al.*, A millifluidic study of cell-to-cell heterogeneity in growth-rate and cell-division capability in populations of isogenic cells of Chlamydomonas reinhardtii, *PLoS One*, 2015, **10**(3), 1–28.
213 E. T. C. Vogt and B. M. Weckhuysen, Fluid catalytic cracking: recent developments on the grand old lady of zeolite catalysis, *Chem. Soc. Rev.*, 2015, **44**(20), 7342–7370.
214 C. Cottin, H. Bodiguel and A. Colin, Influence of wetting conditions on drainage in porous media: A microfluidic study, *Phys. Rev. E: Stat., Nonlinear, Soft Matter Phys.*, 2011, **84**(2), 1–8.
215 C. Odier, B. Levaché, E. Santanach-Carreras and D. Bartolo, Forced Imbibition in Porous Media: A Fourfold Scenario, *Phys. Rev. Lett.*, 2017, **119**(20), 1–5.
216 D. Zhang, *et al.* One-step, facile and ultrafast synthesis of phase- and size-controlled Pt–Bi intermetallic nanocatalysts through continuous-flow microfluidics, *J. Am. Chem. Soc.*, 2015, **137**, 6263–6269.

217 L. Zhang, *et al.* Continuous and scalable production of well-controlled noble-metal nanocrystals in milliliter-sized droplet reactors, *Nano Lett.*, 2014, **14**, 6626–6631.

218 V. V. Zhivonitko, V. V. Telkki and I. V. Koptyug, Characterization of microfluidic gas reactors using remote-detection MRI and parahydrogen-induced polarization, *Angew. Chem., Int. Ed.*, 2012, **51**, 8054–8058.

219 S. Ponce, *et al.* Stable immobilization of size-controlled bimetallic nanoparticles in photonic crystal fiber microreactor, *Chem. Eng. Technol.*, 2018, **90**, 653–659.

220 S. Hannemann, *et al.* Distinct spatial changes of the catalyst structure inside a fixed-bed microreactor during the partial oxidation of methane over Rh/Al_2O_3, *Catal. Today*, 2007, **126**, 54–63.

221 E. Gross, *et al. In situ* IR and X-ray high spatial-resolution microspectroscopy measurements of multistep organic transformation in flow microreactor catalyzed by Au nanoclusters, *J. Am. Chem. Soc.*, 2014, **136**, 3624–3629.

222 Z. Zhang, *et al.* Catalysis by metal nanoparticles in a plug-in optofluidic platform: redox reactions of *p*-nitrobenzenethiol and *p*-aminothiophenol, *ACS Catal.*, 2018, **8**, 2443–2449.

223 X. Z. Lin, A. D. Terepka and H. Yang, Synthesis of silver nanoparticles in a continuous flow tubular microreactor, *Nano Lett.*, 2004, **4**, 2227–2232.

224 H. Zhang, J. J. Wang, J. Fan and Q. Fang, Microfluidic chip-based analytical system for rapid screening of photocatalysts, *Talanta*, 2013, **116**, 946–950.

225 Y. Li, B. Lin, L. Ge, H. Guo, X. Chen and M. Lu, Real-time spectroscopic monitoring of photocatalytic activity promoted by graphene in a microfluidic reactor, *Sci. Rep.*, 2016, **6**, 1–9.

226 Q. Zhang, Q. Zhang, H. Wang and Y. Li, A high efficiency microreactor with Pt/ZnO nanorod arrays on the inner wall for photodegradation of phenol, *J. Hazard. Mater.*, 2013, **254–255**, 318–324.

227 W. Chen, *et al.* Asphaltenes dissolution mechanism study by *in situ* Raman characterization of a packed-bed microreactor with HZSM-5 Aluminosilicates, *Energy Fuels*, 2018, **32**, 12205–12217.